Functional avidity of anti-B7H3 CAR-T constructs predicts antigen density thresholds for triggering effector function

Marta Barisa[1,***], Elisa Zappa [2,6], Henrike Muller[1,6], Rivani Shah[1], Juliane Buhl[2,3] Benjamin Draper[1], Courtney Himsworth[1], Chantelle Bowers[1], Sophie Munnings-Tomes[1], Marilena Nicolaidou[1], Sonia Morlando[1], Katie Birley[1], Clara Leboreiro-Babe[1], Alice Vitali[1], Laura Privitera[1], Kyle O'Sullivan[1], Ailsa Greppi[1], Magdalena Buschhaus[4], Mario Barrera Román[2,3], Sam de Blank[2,3], Femke van den Ham[2], Brenna R. van 't Veld[2], Gabrielle Ferry[1], Laura K. Donovan[1], Louis Chesler[5], Jan Molenaar[2], Jarno Drost[2,3], Anne Rios[2,3], Kerry Chester[4], Judith Wienke[2,**] and John Anderson[1,7,*]

Affiliations

[1] Great Ormond Street Institute of Child Health, University College London, UK

[2] Princess Máxima Center for Pediatric Oncology, Utrecht, The Netherlands

[3] Oncode Institute, Utrecht, The Netherlands

[4] Cancer Institute, University College London, UK

[5] The Institute of Cancer Research, UK

[6] Equal contribution

[7] Lead contact

*Corresponding authors

Correspondence to:

j.anderson@ucl.ac.uk, j.wienke-4@prinsesmaximacentrum.nl, m.barisa@ucl.ac.uk

Abstract

Chimeric Antigen receptor T cell (CAR-T) treatments for solid cancers have been compromised by limited expansion and survival in the tumor microenvironment following interaction with antigen-expressing target cells. Using B7H3 as a model antigen with broad clinical applicability, we evaluated the relationship between the antibody/antigen affinity of three clinical candidate binders and the three following functional characteristics: functional avidity, prolonged cytotoxicity in tumoroid re-stimulation assays, and *in vivo* anti-tumoral responses. BEHAV3D video-microscopy assessed distinct CAR-T cell behaviors at single cell resolution. T cell exhaustion did not dictate effector function. Rather, we demonstrated a threshold avidity of CAR-T / tumor cell interaction, characterized by longer cumulative $CD8^+$ CAR-T / tumor target interaction times, and required for adequate CAR-T cell expansion to result in sustained tumor control upon re-challenge. These results provide new insights into design of CAR-T cells for antigen-dim cell targeting, and avoidance of antigen-dim tumor relapse.

Manuscript word count: 6,975

40 **Introduction**

41 Genetic modification of a cancer patients' T cells with Chimeric antigen receptors (CAR-T
42 cells) for adoptive transfer immunotherapy is a rapidly expanding clinical and scientific field.
43 Clinical studies targeting hematological malignancy using adoptively-transferred CAR-T cell
44 therapy have resulted in FDA approvals of CAR-T products for the treatment of leukaemia,
45 lymphoma and myeloma [1]. In contrast, far fewer durable clinical responses attributable to
46 CAR-T cells are reported in solid cancers despite considerable efforts[2]. A major reason for the
47 relative failure of CAR-T cell adoptive transfer in the solid cancer setting is suboptimal T cell
48 functionality, evidenced by a lack of T cell proliferation and persistence. Reasons for this
49 failure can likely be distilled down to inhibitory effects of the tumor microenvironment and
50 inherent failure of CARs to provide optimal signals to the T cell upon target engagement.

51 CARs comprise an antigen-sensing ectodomain, which is typically a single chain variable
52 fragment (scFv) of an antibody, and endodomains that are an amalgamation of ITAM-
53 containing T cell receptor (TCR) signalling domains, most typically the ζ-chain of CD3, and
54 co-stimulatory domains. CAR-T cells thereby commandeer the MHC-unrestricted antigen
55 specificity of a monoclonal antibody and combine it with T cell signalling in a single molecule.
56 The triggering of T cell activity is dependent on the formation of an effective immune synapse
57 with an antigen-positive target cell. Once a productive synapse is formed, signalling occurs
58 through engagement of the CD3ζ and co-stimulatory moieties with proximal signalling
59 molecules, leading to T cell effector functions and a pro-inflammatory response.

60 For example, structural features of the CAR that influence persistence of effector function
61 include hinge and transmembrane components, and choice and orientation of co-stimulatory
62 endodomains. Moreover, certain scFv binders which signal in the absence of antigen
63 contribute to excessive signalling and subsequent T cell dysfunction[3,4]. Studies in CD19-
64 expressing leukaemia have shown that scFv affinity can affect the strength and duration of the
65 immune synapse with consequences for subsequent disease control[5]. The quality and quantity

66 of immune synapse formation are influenced by binder affinity (both on- and off-rate), target
67 antigen density and CAR expression density. Functional avidity (strength of association
68 between a CAR-T cell and its cellular target), is similarly governed by both affinity of interaction
69 and expression levels of CAR and antigen in the interacting cells. A detailed understanding is
70 lacking of how best to select an optimal CAR scFv for solid tumor-targeting CAR-T cells, and
71 how scFv affinity and avidity impact on sustained functionality in solid tumors.

72 To address these challenges, we chose a broadly expressed solid tumor cancer antigen that
73 is targeted in a number of current CAR-T clinical studies in solid tumors. B7H3 is expressed
74 on solid and hematological cancer in the adult and pediatric settings[6,7]. A member of the
75 immunoglobulin superfamily and closely related to PD-L1, B7H3 is enriched on high-grade
76 tumors and expressed at low levels on healthy tissue[8–13]. There are several B7H3 binders that
77 have been or are being progressed to evaluation in clinical trials including MGA271, 376.96
78 and TE9 [7,9,14]. To specifically evaluate the impact of the scFv binding properties on CAR-T
79 function we cloned these three different binders into identical viral backbones. All constructs
80 had a 2nd generation 28ζ endodomain and CD8 hinge and transmembrane format, and hence
81 we set out to determine generalizable relationships between binder properties with CAR-T
82 function rather than evaluate the binders in the context of their optimized formats for clinical
83 studies.

84 Contrary to our expectations based on preceding literature[5,15–17], we found that CAR-T
85 incorporating either of two scFv's that formed high avidity interaction with B7H3-expressing
86 cells mediated superior anti-tumor functionality compared to a low avidity scFv. Both high and
87 low avidity interactions enabled acute cytotoxicity and cytokine production, but only high
88 avidity interactions led to sustained CAR-T proliferation and consequent activity in the re-
89 challenge setting. These differences in scFv-driven functional potential were most evident
90 against B7H3^{med} or B7H3^{dim} targets, the consequence of which was emergence of antigen-
91 dim escape variants with the low avidity binder. We postulate that, in order to mediate tumour

control, B7H3 CAR-T cells need to interact with their target cell with a supra-threshold avidity, sufficient to drive initial activation and proliferation.

Results

MGA271, 376.96 and TE9 scFv's mediate divergent CAR-T responses against in vivo models of solid tumours

MGA271[18], 376.98[19] and TE9[20] scFv's were cloned into a CD8-28ζ 2nd generation CAR format containing a CD8α hinge-transmembrane, and expressed in SFG γ-retroviral vector with an EF1α promoter as described previously[20]. A compact epitope tag, RQR8[21], was co-expressed from the construct to monitor CAR-T transduction efficiency (Figure 1A). Comparable transgene co-expression between the binders was validated by staining the CAR directly with B7H3-His protein (Supplementary Figure 1). Against LAN-1 and Kelly neuroblastoma targets, we observed enhanced CAR-T cytokine production for 28ζ compared to 4-1BBζ endodomain for all the binders, consistent with previous literature including our own data[7,20,22], and which was concurrent with higher checkpoint receptor expression (Supplementary Figure 2). CD28 co-stimulation was, therefore, chosen over 4-1BB.

We first evaluated TE9 *in vivo* performance in an orthotopic, B7H3-positive[23] Med8A model of medulloblastoma in which NOD.Cg-Prkdc scid Il2rg tm1Wjl /SzJ (NSG) mice received intraventricular CAR-T cells 48 hours after orthotopic cerebellar tumor engraftment. Used in these non-stress conditions, TE9-28ζ fully cleared the tumors within a week of CAR-T infusion (Figure 1B). Next, we evaluated the binders MGA271 and 376.96 in the same model but in increased stress conditions of longer tumor engraftment and lower CAR-T cell dose. Here the 376.96-28ζ treatment was curative (Figure 1C) whilst MGA271-28ζ did not significantly improve survival compared with non-transduced (NTD) T cells. This was unexpected, as both CAR-T products were equivalently cytotoxic against Med8A in a single challenge effector: target (E:T) ratio of 1:10 co-culture (Figure 1D). In a repeat experiment of the stress condition

117 Med8A model, TE9-28ζ CAR-T efficacy matched that of 376.96-28ζ CAR-T, with both binders
118 effecting more cures than MGA271-28ζ CAR-T (Supplementary Figure 3).

119 We have previously shown that MGA271, 376.96 and TE9 28ζ scFv CAR-T are equivalent in
120 short-term single challenge cytotoxicity assays against LAN-1 neuroblastoma cells, and that
121 TE9-28ζ CAR-T significantly enhance survival in a difficult-to-treat subcutaneous LAN1 NSG
122 model[20]. We, therefore, evaluated MGA271 and 376.96-28ζ CAR-T in the LAN-1 *in vivo* model
123 (Figure 1E). Intriguingly, in contrast with the Med8A model where differences between binders
124 were apparent, 376.96 and MGA271 binders performed similarly against LAN-1 tumors,
125 extending survival similarly to what was to described for TE9-28ζ[20]. Taken together, different
126 *in vivo* models establish that B7H3 CAR-T functionality can be affected by scFv selection, but
127 in a manner that is dependent on the choice of tumor target.

128 *MGA271 CAR-T have a lower avidity than 376.96 and TE9 CAR-T for B7H3-expressing tumor*
129 *cells*

130 Despite achieving similar high transduction efficiencies with all three binder CARs
131 (Supplementary Figure 1), we noted that MGA271 CAR-T staining with B7H3-his protein was
132 dimmer than that of matched 376.96 and TE9 CAR-T (Figure 2A, Supplementary Figure 4A).
133 We hypothesized that the strength of the different scFvs' binding to target, and its impact on
134 strength of immune synapse might correlate with the differences observed between binders
135 in the Med8A and LAN-1 *in vivo* studies. To test this, we evaluated the strength of cell-to-cell
136 interaction for each of these CAR-T cells with Med8A, LAN-1, SupT1 wild type (SupT1-WT),
137 and SupT1 transduced with 4-Ig human B7H3 (SupT1-B7H3^{hi}), representing a range of
138 antigen expression (Figure 2B). To avoid differences in transduction efficiency biasing avidity
139 measurement, CAR-T of all scFv's were diluted with donor-matched NTD T cells to
140 standardize expression of the RQR8 marker gene (Supplementary Figure 4B).

141 Avidity measurements were carried out using a Lumicks z-Movi Cell Avidity Analyzer, which
142 measures the force (in piconewtons, pN) required to detach a population of effector cells from

143 their targets (Figure 2C). None of the CAR-T bound to B7H3^{neg} SupT1-WT cells, whilst all three
144 bound B7H3^{pos} cells, albeit with different avidities (Figure 2D,E). TE9 and 376.96 scFv CAR-
145 T consistently bound antigen-positive target cells with higher avidity than MGA271 or NTD
146 cells.

147 To investigate the relationship between antibody-to-antigen binding properties, avidity and
148 antigen target density, we measured the antibodies' affinities, as well as target B7H3
149 molecules per cell in the respective target cell lines. Target cells with high B7H3 per cell overall
150 formed higher avidity synapses with CAR-T, although the positive correlation between binding
151 strength and antigen density was more pronounced for TE9 and 376.96 than MGA271 (Figure
152 2F). Binder affinity of binders in IgG1 format for 4-Ig B7H3 was measured using Surface
153 Plasmon Resonance. TE9 had the highest affinity for B7H3 (0.44nM), similar to 376.96
154 (0.69mM) and higher than MGA271 (1.61nM) (Figure 2G, Supplementary Figure 5). It was of
155 interest that TE9 had both the highest on-rate and the highest off-rate, whilst 376.9 had
156 relatively slow on- and off-rate (Figure 2H). Since affinity is the ratio of off- and on-rates,
157 dissociation constant (K_D) values of TE9 and 376.9 were similar. Binder affinity for B7H3
158 correlated with the intensity of staining of CAR-T cells by recombinant B7H3 protein (Figure
159 2I).

160 *Cytotoxic capacity of low-avidity MGA271 CAR-T deteriorates upon rechallenges with B7H3^{dim}*
161 *but not B7H3^{bright} tumors*

162 To examine the impact of CAR-T binding avidity on effector function, the different constructs
163 were assessed against solid tumor target cells that express a range of B7H3 densities. We
164 selected five different B7H3^{pos} target types which were either cell lines or primary neurosphere
165 cultures (defined hereafter as 'tumoroids'), derived from pediatric solid tumors with a broad
166 range of B7H3 antigen densities as determined using QuantiBright beads (Figure 3A).

167 CAR-T cytotoxicity was first evaluated at a range of E:T ratios in single-challenge short-term
168 assays. All binders displayed equivalent effective cytotoxicity against B7H3^{hi} neuroblastoma

169 cell lines LAN-1 and Kelly (Figure 3B), but relative failure of the lower affinity MGA271 binder
170 was seen when targeting the lower B7H3 antigen density neuroblastoma tumoroids at low E:T
171 ratios (≤1:10) (Figure 3C).

172 Capacity of CAR-T constructs to maintain killing on repeat encounter with target cells is
173 essential for their clinical utility. Therefore, CAR-T were re-challenged over a four-week co-
174 culture as illustrated in Figure 3D. Allowing the CAR-T 6 days to effect cytotoxicity, 691-T
175 tumoroids were killed by both low-avidity CAR MGA271 and representative high-avidity CAR
176 376.96 following the first challenge (Figure 3E). However, MGA271 killing dropped drastically
177 after re-challenge and by the third challenge no MGA271-mediated 691-T killing was
178 observed, while high avidity 376.96 CAR-T maintained tumor control, similar to TE9 CAR-T in
179 an independent experiment (Supplementary Figure 6). Using 691-B tumoroids which have
180 lower antigen density, the high avidity binders 376.96 and TE9 completely eliminated targets
181 after a single challenge whilst MGA271 showed no cytotoxicity. All CAR constructs failed
182 against 691-B upon re-challenge (Figure 3E, Supplementary Figure 6). A similar trend was
183 observed for B7H3^{med} 103-T malignant rhabdoid tumoroids. All CARs were cytotoxic against
184 103-T, but the inferiority of MGA271 was the most pronounced upon challenge during the third
185 and final week (Figure 3F,G).

186 Potential explanations for CAR-T failure in repeat stimulation assays is T cell exhaustion or
187 differentiation to terminal effector cells. While we identified upregulation of
188 exhaustion/activation receptors (including PD-1, TIM-3 and LAG-3) on all scFv CAR-T cells
189 following challenge with neuroblastoma targets (Supplementary Figure 2 for Kelly and LAN-1
190 cell lines; Supplementary Figure 7 for 691 tumoroids), these were not consistently different
191 between the different binders, and, therefore, did not appear to account for functional
192 differences between the CAR products. There were similarly no consistent differences
193 between binders in memory markers CD45RA and CCR7, nor activation markers CD25 and
194 CD69 (Supplementary Figure 7). Collating data from the tumoroid co-cultures at 1:10 E:T ratio,
195 the differences in cytotoxicity between binders at low antigen density was pronounced at both

196 initial challenge and re-challenges, and is represented graphically in Figure 3H. At the lowest
197 antigen density (~1,000 molecules per cell for 691-B tumoroids), only the high avidity binders,
198 TE9 and 376.96, were capable of initiating killing at first challenge but failed to sustain
199 cytotoxicity at re-challenge. At ~5,000 molecules per cell or more, all the binders were effective
200 at initial challenge but only the two high avidity binders sustained killing over multiple rounds
201 of stimulation (Figure 3H).

202 The data prompted us to hypothesize that at high antigen density, binders perform similarly
203 because CAR-T signalling for all of them exceeds a threshold for proliferation and cytokine
204 secretion to initiate tumour control. At low antigen density, high avidity interaction is required
205 to exceed this threshold. Therefore, we next evaluated CAR-T effector functions other than
206 cytotoxicity, including IL-2 and IFN-γ production, and CAR-T cell proliferation.

207 *High avidity interaction with target cells drives CAR-T proliferation and thereby sustained*
208 *effector function*

209 To compare activation profiles, we first measured CAR-T cytokine secretion in response to
210 antigen-bright LAN-1 and Kelly neuroblastoma cell lines. Unexpectedly, despite having seen
211 high and equivalent killing of the targets by all three CARs in short-term killing assays (Figure
212 3B), the lower avidity MGA271 produced significantly lower levels of IFN-γ and IL-2 than TE9
213 and 376.96 CAR-T (Figure 4A,B). MGA271 CAR-T cell numbers declined throughout the
214 assay – in a manner that was indistinguishable from NTD T cells, whilst TE9 and 376.96 CAR-
215 T proliferated at each challenge with targets (Figure 4C).

216 The pattern of CAR-T persistence and proliferation in the 691-T or -B neuroblastoma tumoroid
217 re-challenge assays (Figure 4D and E) mirrored the differential cytokine responses of the
218 different binders. MGA271, but not TE9 and 376.96, numbers declined steadily over time –
219 even in conditions where the MGA271 CAR-T had initially mediated high level killing at first
220 challenge such as was seen against 691-T in Figure 3C and E.

221 To evaluate whether B7H3 CAR-T responses to brain tumor targets are similar, we identified
222 three different medulloblastoma models with a range of antigen densities (Figure 5A). All were
223 B7H3^{med} or B7H3^{med-hi}. CAR-T cytotoxicity upon single challenge with these targets was
224 equivalently high across all scFv's at a range of E:T ratios (Supplementary Figure 8). As was
225 the case with the neuroblastoma targets, however, there were differences in antigen induced
226 CAR-T proliferation between the binders. Low avidity MGA271 proliferated significantly less
227 than TE9 or 376.96 CAR-T, at a level that was not significantly greater than that of NTD T cells
228 (Figure 5B). Proliferation for all CARs was proportionate with antigen expression, and the
229 required B7H3 threshold for driving an increase in T cell numbers was higher for MGA271
230 than TE9 and 376.96 (Figure 5C). Linking CAR-T proliferation to avidity measurements from
231 Figure 2 revealed that for both Med8A and LAN-1 targets, avidity appeared predictive of
232 subsequent T cell proliferation (Figure 5D).

233 *High avidity, determined by ScFv affinity and B7H3 antigen density, drives CAR-T activation*

234 To identify the threshold of B7H3 antigen density for binder-dependent CAR-T functionality
235 within the context of the same target cell, we generated a cell line that expresses a range of
236 B7H3 densities by transducing SupT1 cells with 4-Ig B7H3 (Figure 6A). The SupT1 cells were
237 also transduced with a transgene encoding eGFP and luciferase to enable cytotoxicity
238 evaluation by luminescence. Resulting SupT1-B7H3^{range} contained cells with range of B7H3
239 antigen densities from negative to ultra-high (Figure 6B). CAR-T were challenged with SupT1-
240 B7H3^{range} cells at a 1:1 E:T ratio daily for a week to mimic continued exposure to tumor (Figure
241 6C).

242 While all CAR-T cells exhibited some cytotoxicity against SupT1-B7H3^{range} cells, MGA271
243 killing of targets was consistently lower than that of TE9 and 376.96 CAR-T (Figure 6D). Of
244 note, in contrast to previous targets assayed, MGA271 CAR-T kept up sustained, if low-level,
245 killing even following 7 challenges with targets. None of the CAR-T killed control SupT1-WT
246 cells (Supplementary Figure 9A). Substantial 376.96 and TE9 proliferation was seen as target

247 challenge progressed, whilst more modest MGA271 proliferation was observed (Figure 6E).
248 The antigen dependency of the proliferation was demonstrated by the lack of response in the
249 presence of SupT1-WT targets (Supplementary Figure 9B) or unstimulated conditions (Figure
250 6F). TE9 and 376.96 CAR-T produced significantly more IL-2 and IFN-γ than MGA271 after
251 the initial challenge with SupT1-B7H3^{range} targets (Figure 6G).

252 CAR-T / tumor co-cultures were harvested after the 5th challenge, and residual SupT1-
253 B7H3^{range} expression of B7H3 was measured. Figure 6H shows concatenated B7H3
254 expression on GFP-positive SupT1 cells across the CAR groups. While TE9 and 376.96 CAR-
255 T cultures contained few or no residual B7H3-positive targets, MGA271 CAR-exposed SupT1
256 cells maintained a range of B7H3 expression. Compared to the NTD T cell condition, MGA271
257 eliminated only the antigen-high SupT1 targets (Figure 6H,I).

258 We then aimed to determine the relationship between-T effector function (cytokine secretion
259 and proliferation) and CAR avidity. CAR-T fold-proliferation over 5 challenges with targets
260 correlated with IL-2 production at the time of the initial target challenge, though 376.96 CARs
261 were more consistent initial IL-2 producers than TE9 CARs (Figure 6J). The avidity of CAR-T
262 interaction with SupT1-B7H3^{hi} targets shown in Figure 2 correlated with both IL-2 production
263 and proliferation in response to SupT1-B7H3^{range} cells (Figure 6K,L). A similarly strong but
264 inverse correlation was observed between avidity of interaction and the antigen expression on
265 residual SupT1-B7H3^{range} cells following serial re-challenge (Figure 6M). Taken together, the
266 data indicate that for each cell target engaged by a standard CD28ζ CAR-T cell, there is a
267 threshold of avidity required for sufficient cytokine and proliferation response to allow for
268 expansion and effective cytotoxicity on target re-challenge. We next examined the impact of
269 scFv on B7H3 CAR-T functionality at the single cell level.

270 *High 'on-rate' is associated with high CD8^{+} CAR-T / tumoroid contact duration and rapid*
271 *cytotoxicity against B7H3^{dim} targets*

272 BEHAV3D, a multispectral, 3D image-based platform, is designed to live-track the efficacy
273 and mode of action of cellular immunotherapy at the single cell level [24]. BEHAV3D was used
274 to track anti-B7H3 CAR-T functionality over three challenges with 691-B and 691-T tumor
275 targets. Cultures were imaged during the first (day 0) and third (day 7) challenge with targets,
276 and the series of images then processed for CAR-T behavior using a bioinformatic pipeline,
277 developed by Anne Rios and colleagues[24] (the assay setup is illustrated in Figure 7A and B
278 and Supplementary Figure 10). CAR-T cell behavior was tracked across six different
279 parameters, shown in Figure 7B. Video compilations of day 0 and day 7 CAR-T / tumoroid co-
280 cultures can be viewed in Supplementary Videos 1-24.

281 CAR-T/tumoroid interactions leading to tumoroid death was evident for all conditions
282 (representative co-cultures images shown in Figure 7C). In analysis of behaviors against
283 B7H3^{dim} 691-B tumoroids, striking and unexpected differences were seen between the
284 binders, and between CD4^{+} and CD8^{+} T cells. Plotting the cumulative CD8^{+} CAR-T/tumoroid
285 contact since initiation of the day 0 co-culture showed that TE9 and 376.96 CD8^{+} CAR-T spent
286 significantly longer in contact with B7H3^{dim} 691-B tumoroids than MGA271 CD8^{+} CAR-T did
287 (Figure 7D). A summation of total CD8^{+} CAR-T / 691-B contact time during the entire day-0
288 analysis confirmed this difference between binders (Figure 7F). This cumulative contact score
289 correlated with the cytotoxicity of respective binder-CAR-T constructs against these B7H3^{dim}
290 691-B targets in an overnight 1:10 E:T killing assay (Figure 7D, E). In contrast, all CD8^{+} CAR-
291 T showed similar contact time and cytotoxicity with higher antigen density 691-T tumoroids
292 (Figure 7D-F). Analyzing cytotoxicity by detection of organoid death during the imaging (tumor
293 cell conversion from 'yellow' to 'red' in Figure 7C) confirmed the observation that TE9 CAR-T
294 were the most rapid at killing B7H3^{dim} 691-B tumoroids followed by 376.96 and MGA271 CAR-
295 T cells. In contrast, all CAR-T cells were equally rapid at killing 691-T tumoroids of higher
296 antigen density (Figure 7G).

297 There were no differences between binders in terms of the number of new CAR-T contacts
298 during the 800 minute data collection, using either tumoroid model (Supplementary Figure
299 11A). Hence the finding of highest total T cell/tumoroid contact time of the TE9 CD8 CAR-T
300 cells (Figure 7F) implied TE9 was the binder conferring the longest duration of individual
301 contacts. Consistent with this observation, TE9 $CD8^+$ CAR-T cells also showed the lowest
302 displacement distance (Figure 7H) and speed of displacement (Figure 7I). whilst MGA271 had
303 the shortest and 376.96 were intermediate (Figure 7F,H,I). This ranking of tumor interaction
304 duration of TE9 > 376.96 > MGA271 when targeting low antigen density targets correlated
305 with the cytotoxicity, avidity, and binder association rate constant (Supplementary Figure 11B).
306 These data suggest that high avidity binder $CD8^+$ CAR-T cells stay longer in contact with low
307 antigen tumoroids to facilitate more efficient killing.

308 Compared to $CD8^+$ CAR-T cells, $CD4^+$ CAR-T cells showed greater displacement and reduced
309 tumoroid contact, and this was observed in both models of higher and lower antigen density
310 respectively (Figures 7F,H,I). Moreover, in $CD4^+$ CAR-T, the influence of the respective
311 binders on tumoroid contact and displacement was variable, consistent with $CD4^+$ CAR-T cells
312 having a lesser role in tumoroid contact and direct cytotoxicity, as described previously using
313 BEHAV3D analysis[24] (Figure 7F,H,I). While more mobile overall, $CD4^+$ CAR-T cells did not
314 engage in CAR-T / CAR-T interaction more than $CD8^+$ CAR-T cells (Supplementary Figure
315 11C).

316 *Distinct CAR-T cell characteristics revealed by dimensionality reduction of behavioral*
317 *parameters*

318 To extract behavioral patterns and dynamics, the day 0 BEHAV3D tumor challenge imaging
319 data was clustered using UMAP (Supplementary Figure 12A), revealing six CAR-T behavior
320 types: 'tumoroid engagers' (cluster 1), 'multi-taskers' (clusters 2, 3), 'CAR-T engagers'

321 (clusters 4,5) and 'dying T cells' (cluster 6) (Figure 7J). Fitting with the individual cell analysis,
322 the 'tumoroid engager' cluster 1 was relatively enriched in $CD8^+$ cells compared to $CD4^+$ and
323 with higher antigen density 691-T compared with 691-B targets (Figure 7K). Moreover, TE9
324 and 376.96 binder $CD8^+$ T cells consistently exhibited more cluster 1-type tumor engager
325 behavior than MGA271 CAR-T against both tumor targets, and further exhibited more 'multi-
326 tasker' behavior in the 691-B tumoroid co-culture. These differences between binders were
327 less apparent in the $CD4^+$ CAR-T context.

328 CAR-T behavior was then compared between the two analyzed timepoints (day 0 and day 7).
329 Day 7 CAR-T behavior was reduced using UMAP into 7 clusters across the two imaging
330 sessions (Supplementary Figure 12B), which grouped into 'organoid interaction' (clusters A,
331 B, C, D), 'CAR-T interaction (clusters E, F) and cell death (cluster G) (Supplementary Figure
332 12C). Strikingly, no consistent differences between the CAR-T binders or even $CD4^+$ *vs* $CD8^+$
333 T cells remained evident at day 7 (Supplementary Figure 12D). This narrowing of CAR-T
334 phenotype was evident when comparing the trajectory of tumoroid death over the day 0 and
335 day 7 imaging sessions, pooling data from all three binders and target types (Figure 7L). A
336 broad range of tumor killing trajectory was seen at day 0 whilst at day 7 all CARs mediated
337 rapid tumor clearance. This apparent ability of low avidity MGA271 CAR-T to control low
338 antigen density tumor at day 7 is most likely due to artificially resetting the effector to target
339 ratio at each tumor challenge with re-sorted viable CAR-T cells.

340 The dimensionality reduction BEHAV3D analysis reflects the broad conclusion that high
341 avidity of $CD8^+$ T CAR-T cells equips them for longer interactions with low antigen density
342 targets, which facilitates sustained cytotoxic activity. The data supports our hypothesis that
343 the differences in CAR-T functionality seen *in vivo* and *in vitro* assays are caused not by
344 variation in binder-driven functional exhaustion, but rather by the differential ability of the CAR-
345 T constructs to proliferate and engage in serial tumor cytotoxicity.

346 **Discussion**

347 CAR-T cell technology represents a highly promising cancer therapy as exemplified by FDA
348 approvals for several agents in the hemato-oncology field. In solid cancers the pace of
349 development has been slower. The solid cancer environment is immunologically hostile and
350 hypoxic, which limits of capacity of infiltrating CAR-T Cells to engage in the sustained
351 proliferation and cytotoxicity, which is a requirement for shrinking a solid tumor in which the
352 ratio of tumor to CAR-T cells is stacked in favour of the former. CAR-T relative failure is likely
353 compounded by T cell exhaustion, a phenomenon whereby T cells become transcriptionally
354 programmed to hypo-functionality, as a result of repeated antigen stimulation. The capacity to
355 engage in efficient serial killing through repeated successful interactions with tumor cells
356 without inducing T cell exhaustion may be the defining feature of a successful solid cancer
357 CAR-T construct.

358 The CAR-T to tumor interaction encompasses a CAR immune synapse, wherein the initial
359 contact between T cell and tumor is stabilised by the CAR antibody to target antigen binding
360 interaction, which develops into a cluster of engaged CAR constructs[25,26]. Although the
361 biophysical properties of the CAR-T to antigen synapse are not as well characterized as native
362 TCR immune synapses, it is likely that the strength of this interaction as well as the number of
363 target antigens will determine whether the synapse becomes functional; *i.e.* triggers death of
364 the target cell through release of cytolytic granules concomitant with T cell signalling to
365 promote proliferation and cytokine secretion[25,26].

366 Successful formation of a synapse leads to the exclusion of phosphatases (*e.g.* CD45) and
367 the recruitment of src family kinases (*e.g.* lck) resulting in phosphorylation of CD3ζ chain
368 ITAMs within the CAR molecule, and subsequent signalling. An efficient and high-quality CAR-
369 T immune synapse might be one that is strong enough to induce death of the target and short-
370 lived enough to induce a “goldilocks” quantity and quality of T cell signalling that promotes
371 activation without exhaustion. Immune synapse quality is likely affected by the nature of the

372 initiating antibody-to-antigen interaction. Recent progress in CAR-T / target interaction
373 tracking at the single cell level, on platforms such as BEHAV3D[24], has enabled a nascent
374 understanding of the kinetics of immune synapse formation and how synaptic formation
375 dynamics differ between CD4 and CD8 cells. The relationships between the synapse, the
376 binding properties of the CAR scFv's and the effect of synaptic signalling on T cell activation
377 and exhaustion remain poorly understood.

378 Functional avidity is the strength of interaction between a CAR-T cell and its tumor target,
379 which we have measured as the force required to disrupt the interaction. We hypothesized
380 that avidity would be influenced by three factors: the CAR surface expression on CAR-T cells,
381 the target antigen density on the tumor cells, and the affinity of the antibody to antigen
382 interaction at the single molecular interaction scale. We reasoned that this interplay of factors
383 would be such that none of the parameters alone would be predictive of CAR-T response, but
384 the interaction of the three factors to define functional avidity would be the closest predictor of
385 subsequent T cell function. We evaluated the relationship of antibody to antigen biding
386 properties as both affinity (Biacore surface plasmon resonance) and functional avidity
387 (Lumicks) measurements against a range of antigen densities. Two binders of similar affinity
388 (K_D) had quite differing rate constants of association and dissociation with similar avidity (TE9
389 and 376.96), whilst a third of lower affinity also demonstrated low avidity (MGA271).

390 Several previous studies have investigated avidity of CAR-T cells using the Lumicks platform.
391 For example, the group of Maher *et al* studied a range of anti-CD19 binders in the context of
392 leukemia therapy using conventional 2nd generation CARs co-expressing a 4-1BB chimeric
393 costimulatory receptor[27]. Interestingly, intermediate avidity CAR-T were identified to have the
394 greatest *in vivo* capacity to control tumor growth.

395 Using repeat stimulation assays against suspension cells, monolayers and three dimensional
396 tumoroid models to recapitulate the repeat antigenic engagement of the tumor environment,
397 we show that low avidity interaction on first tumor encounter results in a weak cytokine and

398 proliferative response. Weak initial response translates into ultimate failure of expansion and
399 tumor control in stress conditions. In contrast, higher avidity initial interaction in the low antigen
400 density setting results in effective proliferation and serial killing. In the setting of higher antigen
401 density, all CAR-T constructs have sufficiently high avidity initial interaction to induce
402 expansion and serial killing although low avidity MGA271 still ultimately has reduced
403 functionality at the end of serial challenges. Previous studies have identified fast off-rate as
404 linked to more efficient and effective CAR-T control of leukemia[5,15–17] and it is therefore an
405 interesting contrast in our tumoroid studies to note that the quickest construct for tumor control
406 of low antigen density had the longest organoid contact time as well as the fastest on- and off-
407 rates. This apparent discordance might be explained by the multiple cell contacts that single
408 $CD8^+$ CAR-T generate with the multi-cellular tumoroid structures as previously described using
409 BEHAV3D analysis[24]. Here, a more complex and dynamic interaction of an individual $CD8^+$
410 CAR-T cell with multiple tumor cell targets within a 3D structure might explain a more complex
411 relationship between avidity and success in tumor control.

412 Of note, in the current models which extend to seven repeat tumor challenges we have not
413 seen evidence of differences in T cell exhaustion between the three binders. This may be
414 because the repeat antigenic challenges were not sustained long enough and it is also
415 tempting to speculate that a higher affinity antibody / higher avidity CAR-T cell might have
416 induced exhaustion in the same repeat stimulation experiments. All binders evaluated showed
417 only modest increases in TIM-3^+PD-1^+ double-positive cells and little evidence of exhaustion
418 induced by signalling in the absence of antigen (tonic signalling). It will be important in future
419 studies to evaluate whether very high avidity binders and/or tonic signaling binders show
420 relative failure associated with increased exhaustion marker expression.

421 One notable observation was that the TE9 binder, which had similar affinity and avidity to the
422 376.96 binder, had both the highest on-rate and fastest on-rate. To determine if this impacted
423 on the CAR-T / tumor interaction time, we performed BEHAV3D video microscopy analysis.
424 Interestingly, we found that at higher antigen densities there were no difference in dwell time

425 between the binders. In contrast, at low antigen density, the $CD8^+$ 376.96 and TE9 CAR-T
426 cells had longer dwell times than MGA271 CAR-T, which was consistent with both their greater
427 cytotoxicity and the higher displacement score of the MGA271 CAR-T. The fast on- and off-
428 rates (in single molecule Biacore affinity studies) of TE9 appears to translate into longer
429 tumoroid contact, and leads us to speculate that avidity measurements may prove to be of
430 greater predictive value for CAR-T synapse formation characteristics. A further surprising
431 result was the short tumour dwell-time of TE9 $CD4^+$ cells, which appeared to be of less
432 importance in direct cytotoxicity. Further studies are required to confirm these observations
433 with other binders and targets, as well as mechanistic studies to determine the significance of
434 differences in avidity between $CD4^+$ and $CD8^+$ CAR-T cells.

435 B7H3 is an emerging attractive target for cancer immunotherapy due to its bright expression
436 on the surface of a high proportion of cancer cells, its association with poor prognosis, its
437 potential function as an immune regulator, and its relative absence on healthy tissues [28,29].
438 Interestingly, its cancer specificity seems to extend beyond cancer cells in the tumor
439 environment since several lines of evidence point to its expression in a variety of tumor
440 infiltrating cells, such as vascular endothelial cells. Hence, the clinical application may extend
441 beyond cancers in which B7H3 has a role as a driver oncogene. Indeed, its vascular
442 endothelial expression might mitigate tumor heterogeneity being a cause of antigen escape
443 variants which has been a significant consideration diminishing enthusiasm for clinical
444 progression with several alternate antigens. All three of the binders evaluated in this study are
445 of clinical relevance and are being evaluated in a range of clinical trials.

446 There are three important implications of these avidity findings for clinical activity of these
447 respective binders. The first is threshold of antigen density for activation. B7H3 is expressed
448 at low level on some healthy tissues. A lower avidity binder might have optimal activation
449 threshold to distinguish healthy from tumor tissue to avoid on-target off-tumor toxicity.
450 Secondly, the avidity threshold for activation will be affected by the respective signalling
451 characteristics of the CAR. For example, work using the MGA271 binder has shown that

452 substitution of the CD8 hinge and transmembrane regions (H/TM) as evaluated in this paper,
453 for CD28 H/TM, within the context of 41BB-CD3ζ signaling, results is significantly improved
454 function against low antigen density targets[6]. In current clinical trial NCT05474378 (Mackall
455 and colleagues), the configuration is with CD8 hinge/transmembrane with 41BB costimulation.
456 A second recruiting clinical study (SJ-19-0014; St Jude's, USA; DeRenzo *et al*) using MGA271
457 with CD28ζ is deploying an additional 41BBL co-stimulation *in-trans* module[22], whilst trial
458 NCT04185038[14] (Seattle, USA; Vitanza and team) makes use of MGA271 with CD28 H/TM in
459 a 2nd gen 41BB-CD3ζ configuration. Hence, none of the current MGA271 trials are using the
460 configuration in the current paper. Thirdly, higher expression of CAR through use of higher
461 MOI of virus could increase avidity of a given binder against targets. Artificially, we ensured
462 equivalent expression levels to allow fair comparison of avidity effects in relation to target
463 antigen density. Higher expression of CAR might increase avidity and functionality. What
464 seems clear is that all CARs require fine-tuning of binders to identify optimal activation
465 thresholds. Avidity measurements may prove an additional valuable parameter for screening
466 constructs to optimal signalling and activation.

Figures and Figure Legends

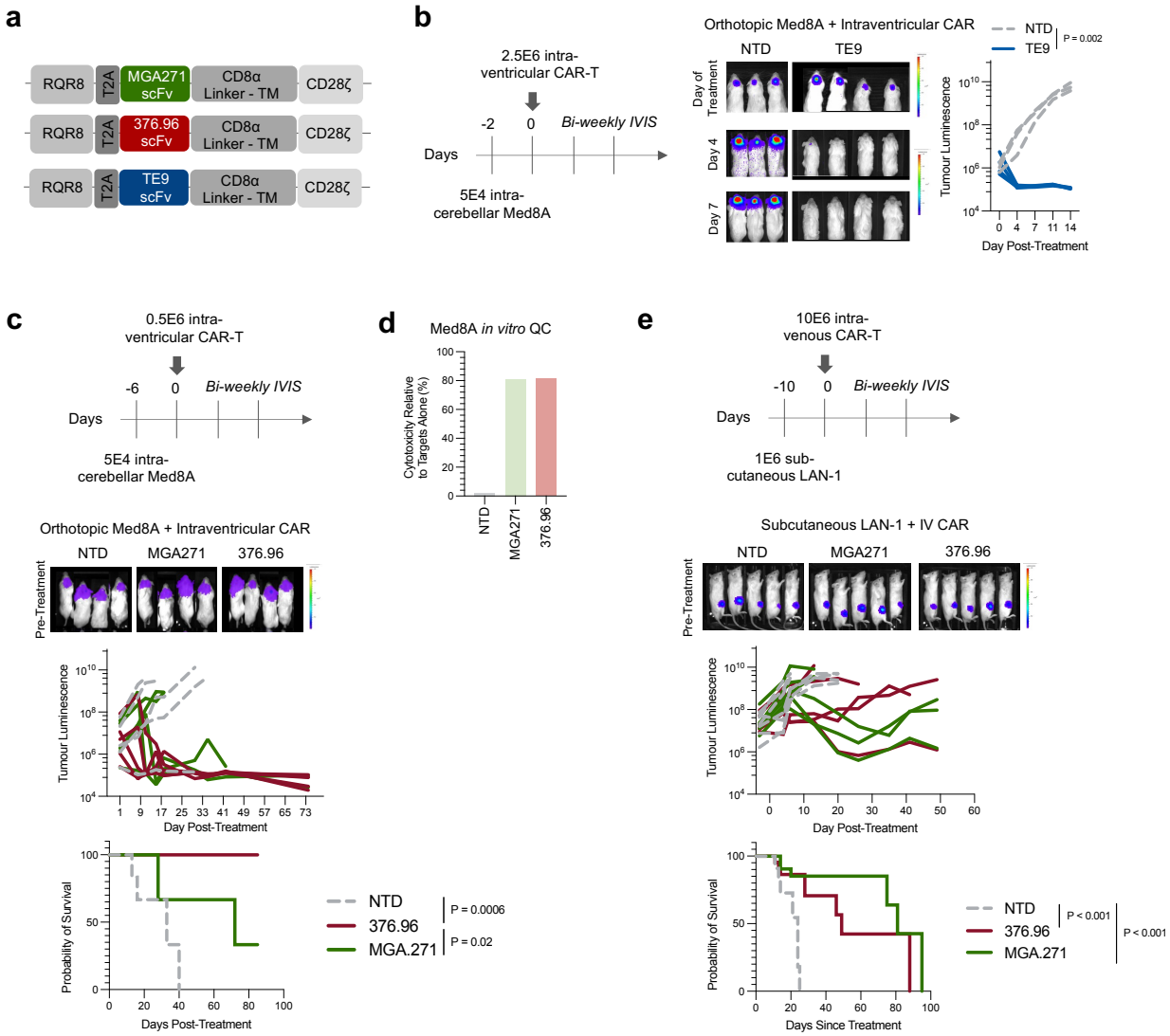

Figure 1. MGA271, 376.96 and TE9 scFv's mediate divergent CAR-T responses against *in vivo* models of medulloblastoma and neuroblastoma. (**A**) Schematic of the retroviral constructs. (**B**) Orthotopic "non-stress" condition Med8A tumor model pilot in NSG mice; N=3 for NTD (non-transduced T cells), N=4 for TE9-CAR (tumor luminescence comparison between groups by Two-Way ANOVA). (**C**) Orthotopic "stress condition" Med8A tumor model in NSG mice; N=4 mice for all conditions (Kaplan-Meyer comparison by Log-rank Mantel-Cox test). (**D**) Overnight CAR-T cytotoxicity assay run in-parallel to the *in vivo* study from panel (**C**) (E:T ratio 1:10, N=1). (**E**) Subcutaneous LAN-1 tumor model in NSG mice. N=5 mice for all conditions (Kaplan-Meyer curve comparison by Log-rank Mantel-Cox test).

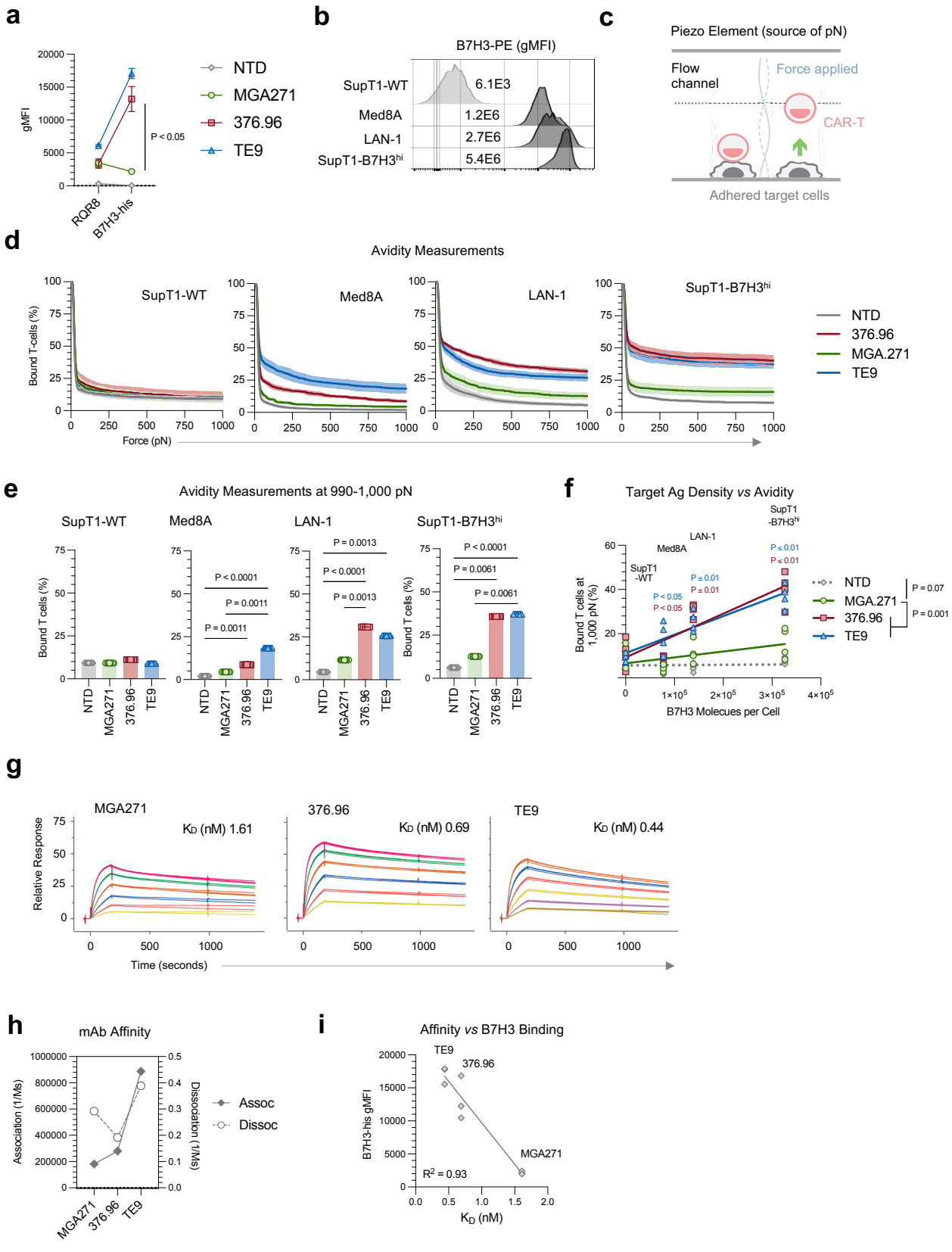

478

479 *Figure 2.* 376.96 and TE9 but not MGA271 CAR-T form high avidity interactions with tumor

480 cells in a B7H3 density dependent manner. (**A**) Cryopreserved, thawed CAR-T cell surface

481 transgene expression was detected using flow cytometry with clone QBEND10 mAb to detect
482 RQR8 marker gene and histidine-x6 tagged B7H3 protein (B7H3-his) + anti-his mAb to detect
483 the CAR (mean ± SEM, N=3 donors, Two-Way ANOVA). (**B**) Target cells were stained with
484 anti-B7H3-PE mAb and analyzed by FACS. Shown on the staggered histogram are respective
485 geometric mean fluorescence intensities (gMFI) of B7H3-PE. (**C**) Principle of Lumicks z-Movi
486 avidity measurement platform. (**D**) CAR-T detachment plotted against force in pN applied to
487 the T cell / target interaction. The line indicates the mean T cell attachment of 4 independent
488 donors across 3 experimental replicates whilst shaded area represents SEM. (**E**) Avidity as
489 represented by attachment at 990-1,000 pN applied force: N=4 donors each with 3
490 experimental replicates, One-Way ANOVA. (**F**) Bound CAR-T (%) at 1,000 pN plotted against
491 QuantiBright defined B7H3 molecules per cell. The lines are linear regressions of the means
492 of 4 individual donors (Two-Way ANOVA). (**G**) Binder affinity for B7H3 (4-Ig) was measured
493 using whole antibodies in IgG1 format using Biacore Surface Plasmon Resonance (SPR). (**H**)
494 The association ('on-rate') and dissociation ('off-rate') rate constants for the different binders
495 were plotted. (**I**) Binder affinity was plotted against the gMFI of B7H3-his protein staining of
496 three independent donor CAR-T cell products.

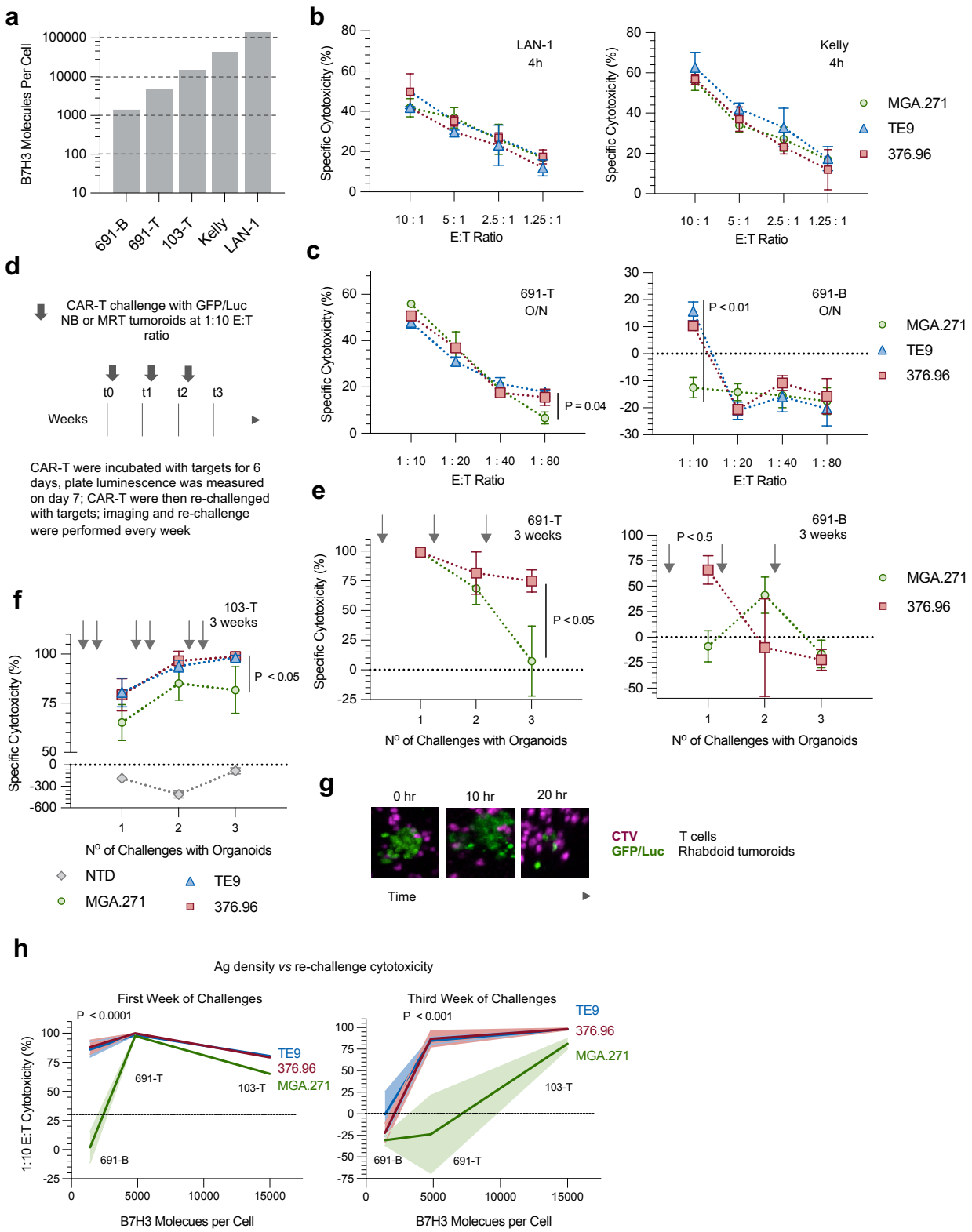

Figure 3. TE9 and 376.96, but not MGA271 CAR-T, respond to B7H3 ultra-dim tumor targets in serial re-challenge cytotoxicity assays. (**A**) Number of B7H3 molecules/cell (QuantiBright flow cytometry assay) for range of targets. (**B**) CAR-T cell cytotoxicity against LAN-1 and Kelly

501 neuroblastoma cell lines (4h ^{51}Cr release assay). 'Specific cytotoxicity' denotes cytotoxicity
502 relative to non-transduced (NTD) T cell controls (mean ± SEM, N=3 donors, Two-Way
503 ANOVA). (**C**) CAR-T cell cytotoxicity against GFP/Luc-engineered tumoroids by overnight
504 luminescence-based assay. 'Specific cytotoxicity' denotes cytotoxicity relative to NTD T cell
505 controls (mean ± SEM, N=2 independent donors across 3 technical replicates, Two-Way
506 ANOVA). (**D-F**) Re-challenge assay timecourse (**D**), against neuroblastoma (**E**) and malignant
507 rhabdoid tumor (MRT) organoids (**F**); gray arrows indicate re-challenge with tumor. In (**E**), data
508 is mean ± SEM, N=2 independent T cell donors across 3 experimental replicates and 'specific
509 cytotoxicity' denotes cytotoxicity relative to NTD T cell controls; in (**F**) 'specific cytotoxicity'
510 denotes cytotoxicity relative to tumor alone controls plated in parallel, data is mean ± SEM,
511 N=1 independent T cell donor (same as one of the donors used to generate data for panel **E**)
512 across 3 experimental replicates. (**G**) Representative microscopy images of 103-T MRT
513 tumoroid being killed by CAR-T over time. (**H**) 1:10 E:T ratio cytotoxicity for the first and third
514 week challenge from the assays showed in panels (**E** and **F**) plotted against antigen density
515 (Quantibright); line = mean cytotoxicity, shaded area = SEM.

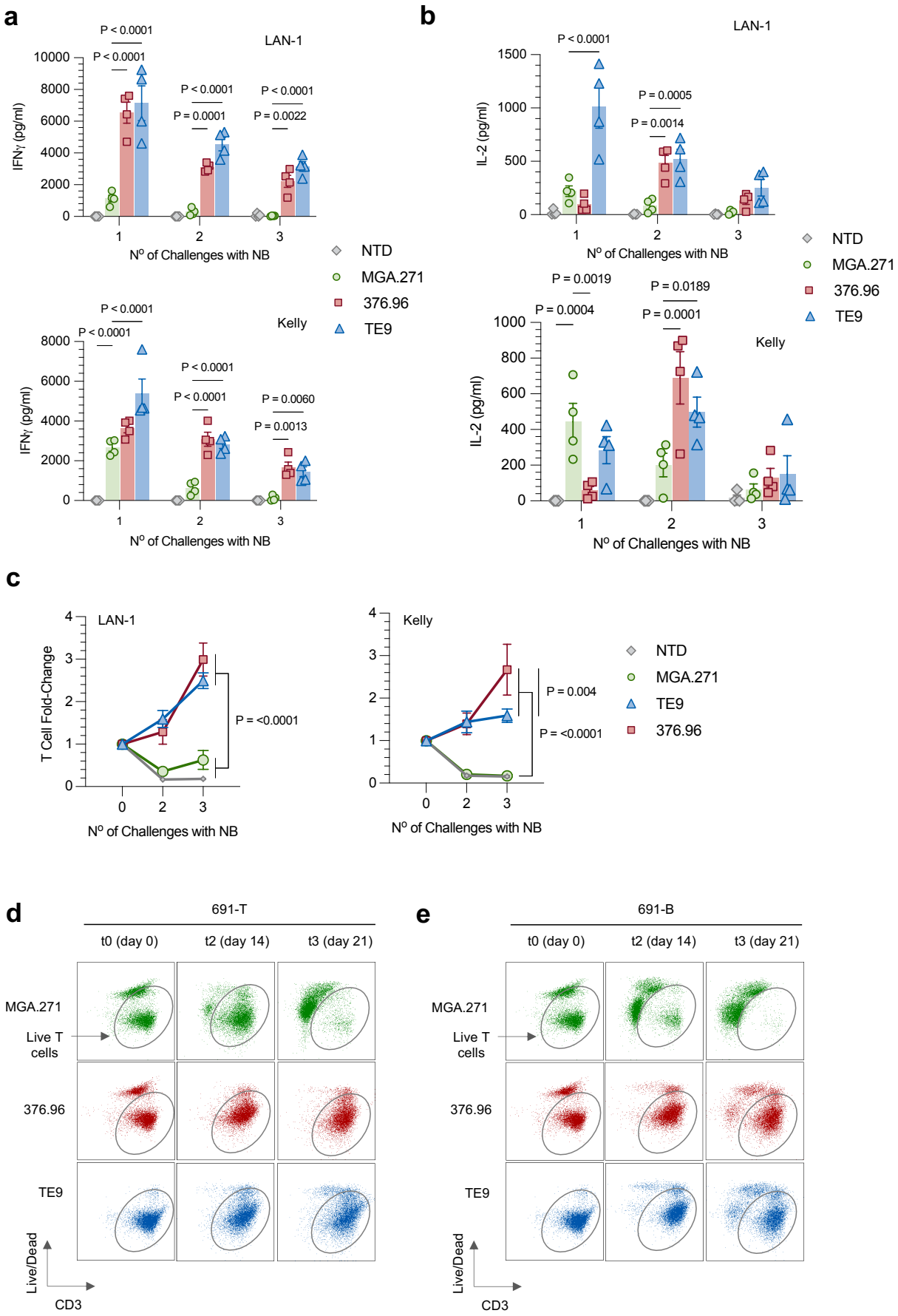
a
LAN-1
IFNγ (pg/ml)
P < 0.0001
P < 0.0001
P < 0.0001
P = 0.0001
P < 0.0001
P = 0.0022
Nº of Challenges with NB
Kelly
P < 0.0001
P < 0.0001
P < 0.0001
P < 0.0001
P = 0.0060
P = 0.0013
b
LAN-1
IL-2 (pg/ml)
P < 0.0001
P = 0.0005
P = 0.0014
Kelly
P = 0.0019
P = 0.0004
P = 0.0189
P = 0.0001
NTD
MGA.271
376.96
TE9
c
LAN-1
T Cell Fold-Change
P = <0.0001
Kelly
P = 0.004
P = <0.0001
d
691-T
t0 (day 0)
t2 (day 14)
t3 (day 21)
MGA.271
Live T cells
376.96
TE9
Live/Dead
CD3
e
691-B

516

517 *Figure 4.* High avidity interaction with target cells drives CAR-T proliferation and resulting
518 sustained effector function. (**A**,**B**) CAR-T cells were stimulated with irradiated LAN-1 or Kelly
519 neuroblastoma cell lines at a 1:1 E:T ratio every 7 days ; IFN-γ (**A**) and IL-2 (**B**) were measured
520 in supernatants collected 24h after every stimulation (mean ± SEM, N=3 independent donors,
521 Two-Way ANOVA). (**C**) T cell numbers in the same co-cultures were evaluated at each time
522 point using Precision Count Beads and flow cytometry (mean ± SEM, N=3 independent
523 donors, Two-Way ANOVA). (**D**) Relative T cell proportions measured using flow cytometry in
524 691-B and 691-T tumor co-cultures over three weeks of weekly tumor challenges at an E:T
525 ratio of 1:10. Gated on singlet PBMC of harvested cultures, representative dot plots from one
526 donor CAR-T are shown.

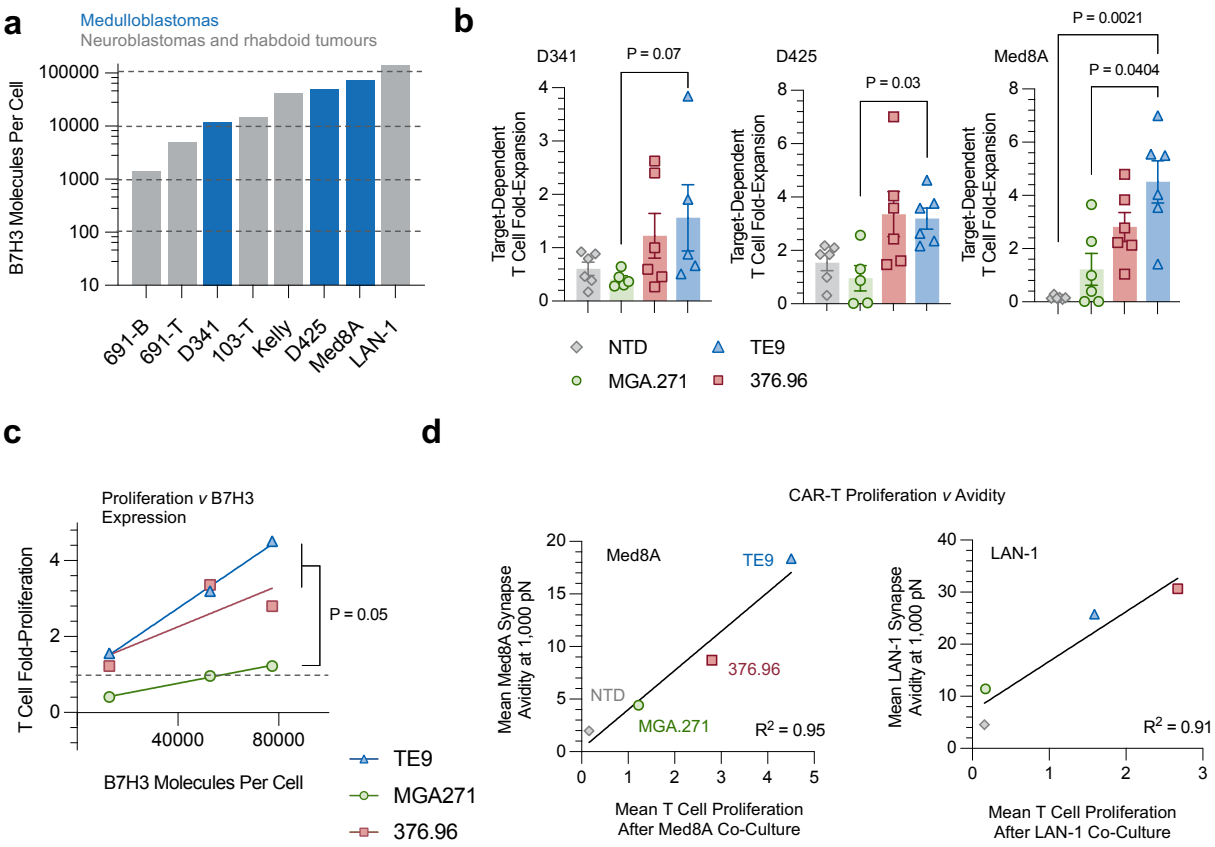

Figure 5. High avidity interactions drive CAR-T proliferation and cytotoxicity in brain tumor models. (**A**) B7H3 molecules per cell were quantified using a QuantiBright flow cytometry assay; brain tumor targets in blue, neuroblastoma and rhabdoid tumor targets in gray. (**B**) T cell proliferation in response to live brain tumor challenge at a 1:1 E:T ratio was quantified after 6 days of co-culture (mean ± SEM, 3 independent T cell donors across two experimental replicates, Kurskal-Wallis test). (**C**) T cell fold-expansion against the number of B7H3 molecules per target cell; dots represent mean proliferation of the different donors and replicates; lines are simple linear regression curves. (**D**) Mean fold-proliferation of CAR-T cells against Med8a and LAN-1 cells was plotted against the mean avidity at 1,000 pN for the two cell lines. The dots represent mean proliferation of the different donors and replicates; the lines are simple linear regression curves.

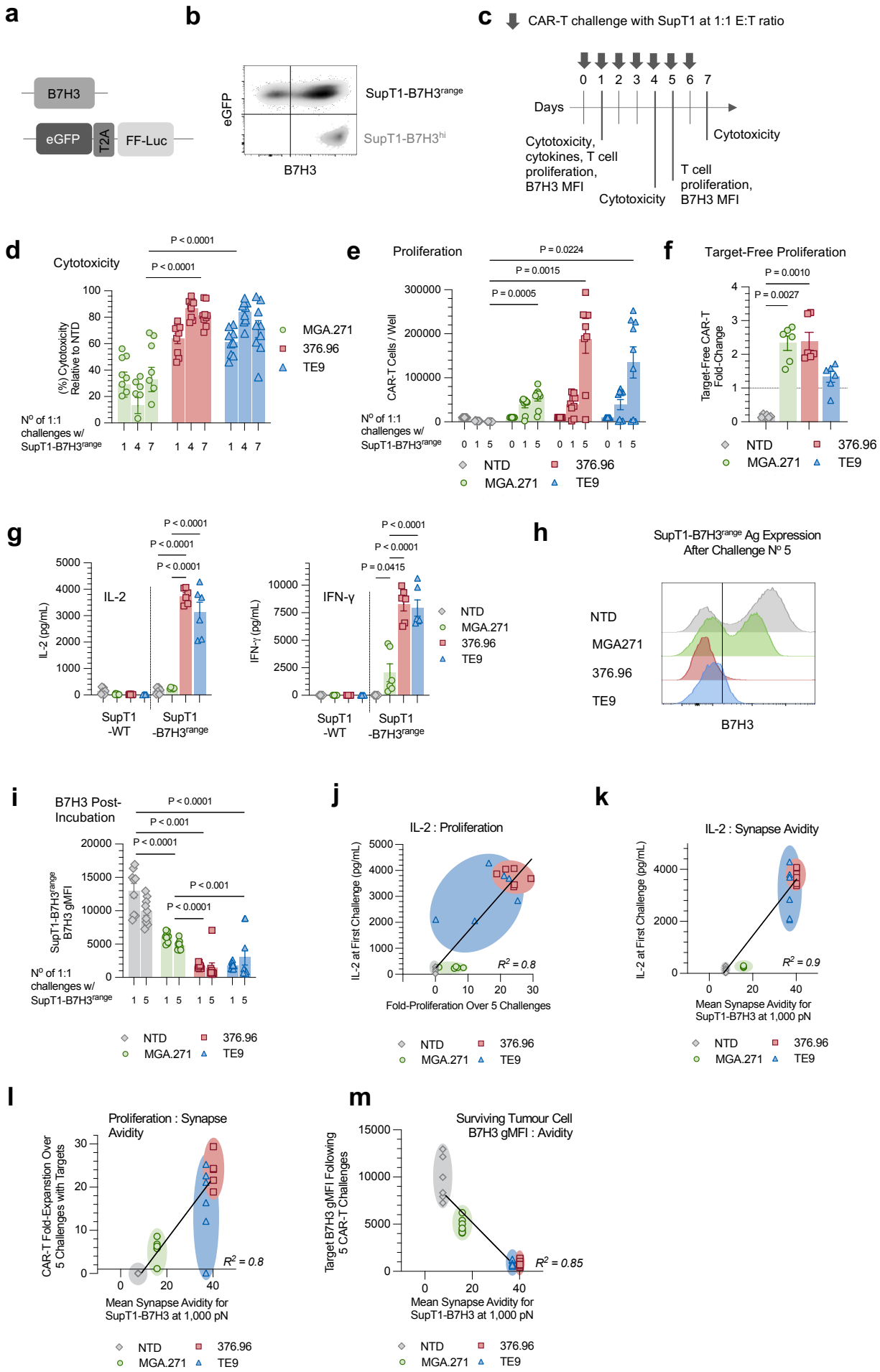
a
B7H3
eGFP
T2A
FF-Luc
b
eGFP
B7H3
SupT1-B7H3range
SupT1-B7H3hi
c
CAR-T challenge with SupT1 at 1:1 E:T ratio
0 1 2 3 4 5 6 7
Days
Cytotoxicity, cytokines, T cell proliferation, B7H3 MFI
Cytotoxicity
T cell proliferation, B7H3 MFI
Cytotoxicity
d
Cytotoxicity
P < 0.0001
P < 0.0001
(%) Cytotoxicity Relative to NTD
Nº of 1:1 challenges w/ SupT1-B7H3range
MGA.271
376.96
TE9
e
Proliferation
P = 0.0224
P = 0.0015
P = 0.0005
CAR-T Cells / Well
Nº of 1:1 challenges w/ SupT1-B7H3range
NTD
376.96
MGA.271
TE9
f
Target-Free Proliferation
P = 0.0010
P = 0.0027
Target-Free CAR-T Fold-Change
NTD
376.96
MGA.271
TE9
g
IL-2
P < 0.0001
P < 0.0001
P < 0.0001
IL-2 (pg/mL)
SupT1 -WT
SupT1 -B7H3range
IFN-γ
P < 0.0001
P < 0.0001
P = 0.0415
IFN-γ (pg/mL)
NTD
MGA.271
376.96
TE9
h
SupT1-B7H3range Ag Expression After Challenge Nº 5
NTD
MGA271
376.96
TE9
B7H3
i
B7H3 Post-Incubation
P < 0.0001
P < 0.001
P < 0.0001
P < 0.001
P < 0.0001
SupT1-B7H3range B7H3 gMFI
Nº of 1:1 challenges w/ SupT1-B7H3range
NTD
376.96
MGA.271
TE9
j
IL-2 : Proliferation
IL-2 at First Challenge (pg/mL)
R2 = 0.8
Fold-Proliferation Over 5 Challenges
NTD
376.96
MGA.271
TE9
k
IL-2 : Synapse Avidity
IL-2 at First Challenge (pg/mL)
R2 = 0.9
Mean Synapse Avidity for SupT1-B7H3 at 1,000 pN
NTD
376.96
MGA.271
TE9
l
Proliferation : Synapse Avidity
CAR-T Fold-Expansion Over 5 Challenges with Targets
R2 = 0.8
Mean Synapse Avidity for SupT1-B7H3 at 1,000 pN
NTD
376.96
MGA.271
TE9
m
Surviving Tumour Cell B7H3 gMFI : Avidity
Target B7H3 gMFI Following 5 CAR-T Challenges
R2 = 0.85
Mean Synapse Avidity for SupT1-B7H3 at 1,000 pN
NTD
376.96
MGA.271
TE9

539

540 *Figure 6.* High avidity drives elimination of antigen-dim targets. (**A**) Constructs for generation
541 of B7H3 and GFP/luciferase sublines of SupT1 cells. (**B**) Expression of B7H3 in the unsorted
542 'SupT1-B7H3^{range}' and flow-sorted 'SupT1-B7H3^{hi}' cells. (**C**) Rechallenge assay experimental
543 schematic. For all subsequent data in the panels: N=4 independent donors across 4
544 experimental replicates. (**D**) Cytotoxicity was measured by luciferase signal as relative to
545 tumor luminescence in the presence of donor-matched non-transduced (NTD) T cells (mean
546 ± SEM, Two-Way ANOVA). (**E**) T cell numbers in the same assay following either a range of
547 challenges with tumor targets or (**F**) target-free (mean ± SEM, Two-Way ANOVA). (**G**)
548 Cytokine measurements in co-culture supernatants following a single challenge wit SupT1-
549 B7H3^{range} targets at a 1:1 E:T ratio (mean ± SEM, Two-Way ANOVA). (**H**) B7H3 expression
550 on targets was measured using flow cytometry following the fifth challenge. Shown are
551 concatenated histograms that were generated by combining flow data adjusted for 10,000
552 SupT1 cells per sample. (**I**) The same SupT1-B7H3^{range} positivity for antigen as analysed in
553 each sample separately (mean represents geometric mean fluorescence intensity (gMFI) ±
554 SEM, Two-Way ANOVA). (**J**) Respective CAR fold-proliferation in response to 5 challenges
555 with SupT1-B7H3^{range} targets plotted against IL-2 production following the initial challenge. (**K**)
556 IL-2 production after first challenge plotted against the mean avidity for SupT1-B7H3^{hi} targets
557 at 1,000 pN. (**L**) Proliferation after 5 challenges with targets was plotted against the mean
558 synapse avidity that the respective CARs achieved when combined with SupT1-B7H3^{hi} targets
559 at 1,000 pN. (**M**) SupT1-B7H3^{range} cell B7H3 gMFI after 5 challenges with targets was plotted
560 against the mean synapse avidity that the respective CARs achieved when combined with
561 SupT1-B7H3^{hi} targets at 1,000 pN. In (**J**-**M**) each dot represents an individual donor
562 experimental replicate, the lines are simple linear regressions.

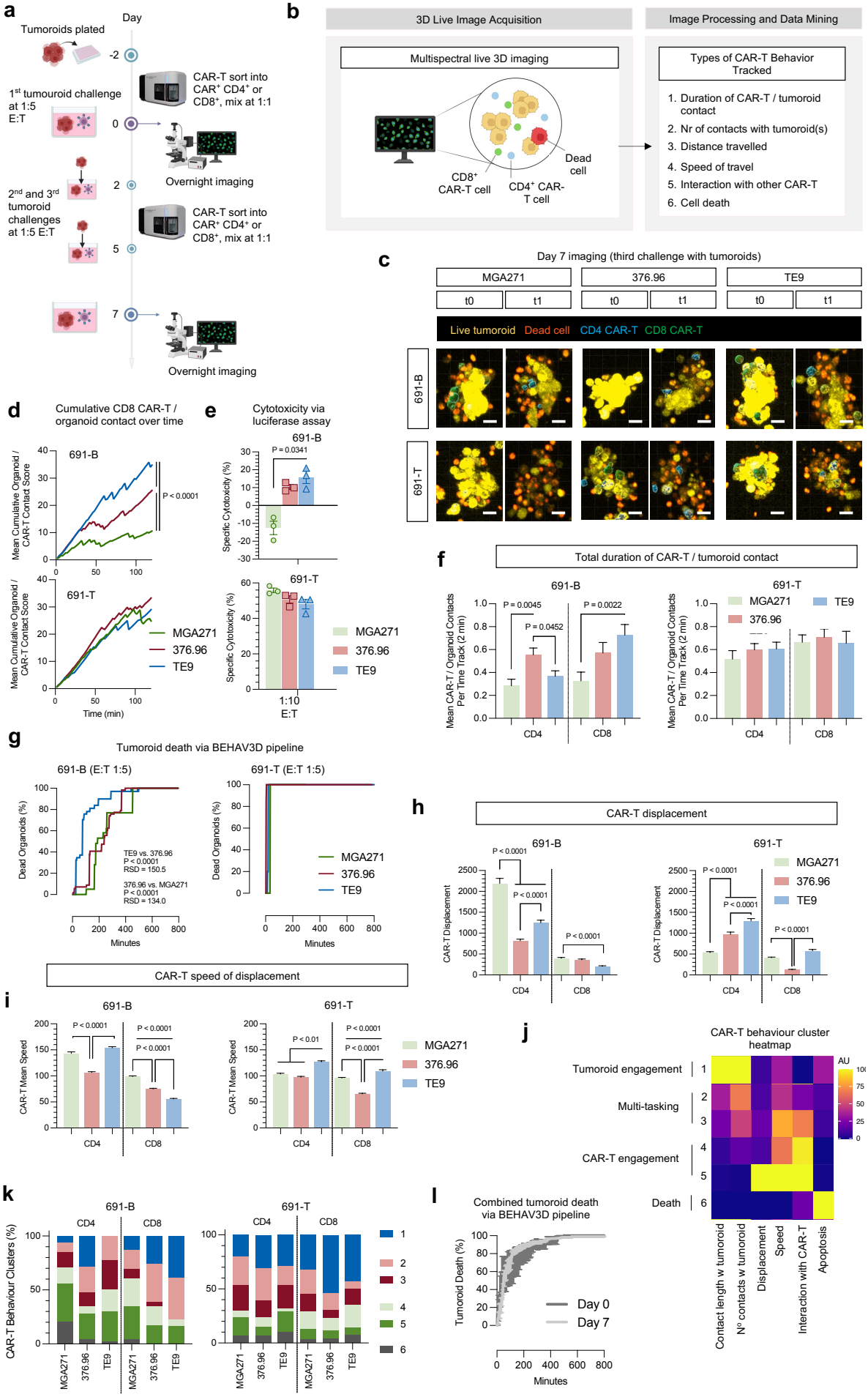
a
Day
Tumoroids plated
-2
1st tumouroid challenge at 1:5 E:T
CAR-T sort into CAR+ CD4+ or CD8+, mix at 1:1
0
Overnight imaging
2nd and 3rd tumoroid challenges at 1:5 E:T
2
CAR-T sort into CAR+ CD4+ or CD8+, mix at 1:1
5
7
Overnight imaging
b
3D Live Image Acquisition
Image Processing and Data Mining
Multispectral live 3D imaging
CD8+ CAR-T cell
CD4+ CAR-T cell
Dead cell
Types of CAR-T Behavior Tracked
1. Duration of CAR-T / tumoroid contact
2. Nr of contacts with tumoroid(s)
3. Distance travelled
4. Speed of travel
5. Interaction with other CAR-T
6. Cell death
c
Day 7 imaging (third challenge with tumoroids)
MGA271
376.96
TE9
t0
t1
Live tumoroid
Dead cell
CD4 CAR-T
CD8 CAR-T
691-B
691-T
d
Cumulative CD8 CAR-T / organoid contact over time
Mean Cumulative Organoid / CAR-T Contact Score
691-B
691-T
P < 0.0001
MGA271
376.96
TE9
Time (min)
e
Cytotoxicity via luciferase assay
Specific Cytotoxicity (%)
P = 0.0341
1:10
E:T
f
Total duration of CAR-T / tumoroid contact
Mean CAR-T / Organoid Contacts Per Time Track (2 min)
P = 0.0045
P = 0.0452
P = 0.0022
CD4
CD8
g
Tumoroid death via BEHAV3D pipeline
691-B (E:T 1:5)
691-T (E:T 1:5)
Dead Organoids (%)
TE9 vs. 376.96
P < 0.0001
RSD = 150.5
376.96 vs. MGA271
P < 0.0001
RSD = 134.0
Minutes
h
CAR-T displacement
CAR-T Displacement
P < 0.0001
i
CAR-T speed of displacement
CAR-T Mean Speed
P < 0.01
j
CAR-T behaviour cluster heatmap
Tumoroid engagement
Multi-tasking
CAR-T engagement
Death
AU
Contact length w tumoroid
Nº contacts w tumoroid
Displacement
Speed
Interaction with CAR-T
Apoptosis
k
CAR-T Behaviour Clusters (%)
l
Combined tumoroid death via BEHAV3D pipeline
Tumoroid Death (%)
Day 0
Day 7

563

564 *Figure 7.* Higher CAR binder B7H3 avidity associated with increased $CD8^+$ CAR-T / tumoroid
565 contact duration and more rapid cytotoxicity against $B7H3^{ultra\text{-}dim}$ tumoroids. (**A**,**B**) experimental
566 overview. (**C**) Illustrative stills of tumoroid and T cell clusters at the start (day 0 = t0), and end
567 (day 7 = t1) 800 minute imaging sessions. (**D**) $CD8^+$ CAR-T cell cumulative contact time with
568 691-B and 691-T organoids tracked for the first 2h of the first tumor challenge on day 0. The
569 line represents the mean cumulative tumoroid contact score of all the individual CAR-T cells
570 that were successfully tracked for the full 120 min period (the number of cells tracked in each
571 of the conditions was a mean 31.33±10.8; curves were compared using simple linear
572 regressions). (**E**) CAR-T cells were incubated with tumoroids overnight at a 1:10 E:T ratio.
573 'Specific cytotoxicity' denotes tumor luminescence relative to matched non-transduced T cell
574 (NTD) controls (mean ± SEM, N=3 independent experimental replicates, Kruskal-Wallis test).
575 **(F-I)** Respective parameters were tracked for entire duration (800 minutes) of the first tumor
576 challenge at day 0. (**F**) $CD4^+$ and $CD8^+$ CAR-T cell cumulative contact time with 691-B and
577 691-T organoids (mean ± SEM, N = 31.5 ± 10.6 cells per T cell condition, Two-Way ANOVA).
578 (**G**) Cumulative tumoroid death (conversion from viability dye yellow to red) (a total of 398
579 incremental time-points were recorded to track tumoroid apoptosis over the assay; curve
580 comparison was carried out using a Friedman test for P value and rank sum differences
581 (RSD)). (**H**) $CD4^+$ and $CD8^+$ CAR-T displacement (mean ± SEM, N = 31.5 ± 10.6 cells per T
582 cell condition, Two-Way ANOVA). (**I**) Mean speed of $CD4^+$ and $CD8^+$ CAR-T displacement
583 (mean ± SEM, N = 31.5 ± 10.6 cells per T cell condition, Two-Way ANOVA). (**J**) Trends in
584 CAR-T behavior reduced into 6 clusters using UMAP analysis of the T cell behavior across all
585 the conditions observed in the initial tumor challenge at day 0 and represented as a heatmap.
586 (**K**) The CAR-T behaviors broken down by T cell, binder and target type. (**L**) Pooled data from
587 all CAR constructs against both targets comparing day 0 and day 7 challenge rate of organoid
588 death.

589 **Acknowledgements**

590 We thank Debarati Shome and Reza Nadafi of Lumicks for their support with our z-Movi
591 analysis of B7H3-CAR-T synapse avidities, and Lumicks more broadly for supporting us with
592 hardware and technical advice during the experiments. We're grateful to the Flow Cytometry
593 Core Facility at UCL GOS Institute of Child Health and to the Imaging Center at the Princess
594 Máxima Center for their support in running our studies. We thank the Princess Máxima Center
595 Imaging and Tumoroid facilities for support.

596 **Funding**

597 We are grateful for the following grant support. Anderson and Chesler: Stand up to Cancer/
598 CRUK Paediatric Cancer New Discoveries Challenge; Anderson, Chesler and Donovan: CwC
599 INSTINCT-MB award, Fight Kids Cancer, and LPT programme awards; Anderson: Research
600 into Childhood Cancer, NIHR GOSH BRC, GOSHCC 552864, AMR/LifeArc awards. Drost and
601 Buhl: Oncode Institute, Children Cancer-free Foundation (KiKa), Deutsche
602 Forschungsgemeinschaft (German Research Foundation, DFG). Molenaar: Villa Joep, Veni.

603 **Author Contributions**

604 MB, JW, and JA wrote the manuscript; MB, HM, EZ, MBR, and SbD analyzed data; GF
605 generated reagents; EZ, HM, RS, BD, CH, CB, SMT, MN, SM, KB, CLB, AV, LP, KoS, AG,
606 and MB performed experiments; JA, JW, JB, KC, AR, JD, JM, LC co-supervised the research.

607 **Conflicts of Interest**

608 MB, JA, KC, KB, MB hold patents in CAR-T technology development, including a pending
609 patent for the TE9 anti-B7H3 binder. JA holds founders shares in Autolus.

610 **References**

611

612 1. Research, C. for B. E. and. Approved Cellular and Gene Therapy Products. *FDA* (2023).

613 2. Albelda, S. M. CAR T cell therapy for patients with solid tumours: key lessons to learn and
614 unlearn. *Nat Rev Clin Oncol* **21**, 47–66 (2024).

615 3. Weber, E. W. *et al.* Transient "rest" restores functionality in exhausted CAR-T cells via
616 epigenetic remodeling. *Science* **372**, eaba1786 (2021).

617 4. Weber, E. W. *et al.* Pharmacologic control of CAR-T cell function using dasatinib. *Blood*
618 *Adv* **3**, 711–717 (2019).

619 5. Ghorashian, S. *et al.* Enhanced CAR T cell expansion and prolonged persistence in
620 pediatric patients with ALL treated with a low-affinity CD19 CAR. *Nature Medicine* **25**,
621 1408–1414 (2019).

622 6. Majzner, R. G. *et al.* Tuning the Antigen Density Requirement for CAR T-cell Activity.
623 *Cancer Discov* **10**, 702–723 (2020).

624 7. Du, H. *et al.* Antitumor Responses in the Absence of Toxicity in Solid Tumors by
625 Targeting B7-H3 via Chimeric Antigen Receptor T Cells. *Cancer Cell* **35**, 221-237.e8
626 (2019).

627 8. Theruvath, J. *et al.* Locoregionally administered B7-H3-targeted CAR T cells for treatment
628 of atypical teratoid/rhabdoid tumors. *Nat Med* **26**, 712–719 (2020).

629 9. Majzner, R. G. *et al.* CAR T Cells Targeting B7-H3, a Pan-Cancer Antigen, Demonstrate
630 Potent Preclinical Activity Against Pediatric Solid Tumors and Brain Tumors. *Clinical*
631 *Cancer Research* **25**, 2560–2574 (2019).

632 10. Maachani, U. B. *et al.* B7-H3 as a Prognostic Biomarker and Therapeutic Target in
633 Pediatric central nervous system Tumors. *Transl Oncol* **13**, 365–371 (2020).

634 11. Modak, S., Kramer, K., Gultekin, S. H., Guo, H. F. & Cheung, N. K. Monoclonal
635 antibody 8H9 targets a novel cell surface antigen expressed by a wide spectrum of
636 human solid tumors. *Cancer Res* **61**, 4048–4054 (2001).

637 12. Chapoval, A. I. *et al.* B7-H3: A costimulatory molecule for T cell activation and IFN-γ
638 production. *Nature Immunology* **2**, 269–274 (2001).
639 13. Wang, L., Kang, F.-B. & Shan, B.-E. B7-H3-mediated tumor immunology: Friend or
640 foe? *International Journal of Cancer* **134**, 2764–2771 (2014).
641 14. Vitanza, N. A. *et al.* Intraventricular B7-H3 CAR T Cells for Diffuse Intrinsic Pontine
642 Glioma: Preliminary First-in-Human Bioactivity and Safety. *Cancer Discov* **13**, 114–131
643 (2023).
644 15. Chmielewski, M., Hombach, A., Heuser, C., Adams, G. P. & Abken, H. T Cell
645 Activation by Antibody-Like Immunoreceptors: Increase in Affinity of the Single-Chain
646 Fragment Domain above Threshold Does Not Increase T Cell Activation against Antigen-
647 Positive Target Cells but Decreases Selectivity1. *The Journal of Immunology* **173**, 7647–
648 7653 (2004).
649 16. Mause, E. R. V. *et al.* Combinatorial T cell engineering eliminates on-target off-tumor
650 toxicity of CD229 CAR T cells while maintaining anti-tumor activity. 2021.12.06.471279
651 Preprint at https://doi.org/10.1101/2021.12.06.471279 (2022).
652 17. Olson, M. L. *et al.* Low-affinity CAR T cells exhibit reduced trogocytosis, preventing
653 rapid antigen loss, and increasing CAR T cell expansion. *Leukemia* **36**, 1943–1946
654 (2022).
655 18. Loo, D. *et al.* Development of an Fc-enhanced anti-B7-H3 monoclonal antibody with
656 potent antitumor activity. *Clin Cancer Res* **18**, 3834–3845 (2012).
657 19. Imai, K., Wilson, B. S., Bigotti, A., Natali, P. G. & Ferrone, S. A 94,000-dalton
658 glycoprotein expressed by human melanoma and carcinoma cells. *J Natl Cancer Inst* **68**,
659 761–769 (1982).
660 20. Birley, K. *et al.* A novel anti-B7-H3 chimeric antigen receptor from a single-chain
661 antibody library for immunotherapy of solid cancers. *Molecular Therapy - Oncolytics* **26**,
662 429–443 (2022).
663 21. Philip, B. *et al.* A highly compact epitope-based marker/suicide gene for easier and
664 safer T-cell therapy. *Blood* **124**, 1277–1287 (2014).

665 22. Nguyen, P. *et al.* Route of 41BB/41BBL Costimulation Determines Effector Function
666 of B7-H3-CAR.CD28ζ T Cells. *Mol Ther Oncolytics* **18**, 202–214 (2020).
667 23. Labanieh, L. *et al.* Enhanced safety and efficacy of protease-regulated CAR-T cell
668 receptors. *Cell* **185**, 1745-1763.e22 (2022).
669 24. Dekkers, J. F. *et al.* Uncovering the mode of action of engineered T cells in patient
670 cancer organoids. *Nat Biotechnol* 1–10 (2022) doi:10.1038/s41587-022-01397-w.
671 25. Sajman, J. *et al.* Nanoscale CAR Organization at the Immune Synapse Correlates
672 with CAR-T Effector Functions. *Cells* **12**, 2261 (2023).
673 26. Xiong, Y., Libby, K. A. & Su, X. The physical landscape of CAR-T synapse.
674 *Biophysical Journal* (2023) doi:10.1016/j.bpj.2023.09.004.
675 27. Halim, L. *et al.* Engineering of an Avidity-Optimized CD19-Specific Parallel Chimeric
676 Antigen Receptor That Delivers Dual CD28 and 4-1BB Co-Stimulation. *Frontiers in*
677 *Immunology* **13**, (2022).
678 28. Kontos, F. *et al.* B7-H3: An Attractive Target for Antibody-based Immunotherapy.
679 *Clinical Cancer Research* **27**, 1227–1235 (2021).
680 29. Zhou, W.-T. & Jin, W.-L. B7-H3/CD276: An Emerging Cancer Immunotherapy.
681 *Frontiers in Immunology* **12**, (2021).
682 30. Schutgens, F. *et al.* Tubuloids derived from human adult kidney and urine for
683 personalized disease modeling. *Nat Biotechnol* **37**, 303–313 (2019).
684 31. Calandrini, C. *et al.* An organoid biobank for childhood kidney cancers that captures
685 disease and tissue heterogeneity. *Nat Commun* **11**, 1310 (2020).
686 32. Custers, L. *et al.* Somatic mutations and single-cell transcriptomes reveal the root of
687 malignant rhabdoid tumours. *Nat Commun* **12**, 1407 (2021).
688 33. Koo, B.-K. *et al.* Controlled gene expression in primary Lgr5 organoid cultures. *Nat*
689 *Methods* **9**, 81–83 (2011).
690 34. Johnson, L. S., Huang, L., Moore, P. A., Loo, D. T. & Chen, F. Z. Antibodies reactive
691 with B7-H3 and uses thereof. (2014).

692 35. Dotti, G., Ferrone, S., Du, H., Wang, X. & Ferrone, C. Methods and compositions for
693 chimeric antigen receptor targeting cancer cells. (2019).
694 36. Sabbatino, F. *et al.* Novel Tumor Antigen-Specific Monoclonal Antibody-Based
695 Immunotherapy to Eradicate Both Differentiated Cancer Cells and Cancer-Initiating Cells
696 in Solid Tumors. *Seminars in Oncology* **41**, 685–699 (2014).
697 37. The z-Movi Cell Avidity Analyzer workflow. *LUMICKS*
698 https://lumicks.com/knowledge/the-z-movi-workflow/.
699 38. Jason-Moller, L., Murphy, M. & Bruno, J. Overview of Biacore systems and their
700 applications. *Curr Protoc Protein Sci* **Chapter 19**, Unit 19.13 (2006).

701

702 **Methods**

703 *Cells lines and culture conditions*

704 All cell lines were cultured in humidified 37C° in 5% CO_2 conditions. Cell lines were thawed
705 and passaged for at least two weeks prior to use in functional assays. Culture mycoplasma
706 tests were performed monthly using MycoAlert Detection Kit from Lonza. The following table
707 summarizes the characteristics and culture conditions of the cell lines that were used over the
708 course of this study.

709

Cell Line ID	***Type of Cancer***	***Source***	***RRID***	***Culture Media***
LAN-1 (LA-N-1)	Neuroblastoma	ECACC	CVCL_1827	RPMI1640 (Gibco) + 10% FCS (Gibco)
Med8A (MED-MEB-8A) wild type	Medulloblastoma	Gift from Michael Taylor, The Hospital for Sick Children, Canada	CVCL_M137	DMEM (Gibco) + 10% FCS + 1x Glutamax (Gibco)
Med8A GFP/Luc	Medulloblastoma	Derived from Med8A wild type by RD114 γ-retroviral transduction with GFP/Luc	None	DMEM (Gibco) + 10% FCS + 1x Glutamax (Gibco)
Kelly	Neuroblastoma	Gift from Andrew Stoker, UCL, UK	CVCL_2092	RPMI1640 + 10% FCS
SupT1 wild type	Childhood T lymphoblastic lymphoma	ECACC	CVCL_1714	RPMI1640 + 10% FCS
SupT1-B7H3^{hi}	Childhood T lymphoblastic lymphoma	Derived from SupT1 wild type by RD114 γ-retroviral transduction with 4-Ig B7H3 (Sinobiological), followed by flow cytometric sorting	None	RPMI1640 + 10% FCS
SupT1-B7H3^{range} GFP/Luc	Childhood T lymphoblastic lymphoma	Derived from SupT1 wild type by RD114 γ-retroviral transduction with GFP/Luc followed by flow cytometric sorting, then 4-Ig B7H3 (Sinobiological) without sorting	None	RPMI1640 + 10% FCS

691-T (AMC691-T) wild type	Neuroblastoma	Gift from Jan Molenaar (Utrecht)	None	'Neurosphere medium': DMEM-GlutaMAX supplemented with 20% Ham's F-12 nutrient mixture, 2% B-27 supplement minus vitamin A, 1% N-2 Supplement, 100 U/mL penicillin, 100 mg/mL streptomycin, 300 ng/mL insulin-like growth factor (IGF-1), 40 ng/mL fibroblast growth factor-basic (FGF-2), 20 ng/mL epidermal growth factor (EGF), 10 ng/mL platelet-derived growth factor-AA (PDGF-AA) and 10 ng/mL platelet-derived growth factor-BB (PDGF-BB)
691-T (AMC691-T) GFP/Luc	Neuroblastoma	Gift from Jan Molenaar (Utrecht)	None	'Neurosphere medium'
691-B (AMC691-B)	Neuroblastoma	Gift from Jan Molenaar (Utrecht)	None	'Neurosphere medium'
691-B (AMC691-B) GFP/Luc	Neuroblastoma	Gift from Jan Molenaar (Utrecht)	None	'Neurosphere medium'
103-T wild type	Malignant rhabdoid tumor	Gift from Jarno Drost (Utrecht)	None	'MRT medium'[30,31]: MRT tumoroids were cultured in droplets of growth factor-reduced basement membrane extract (BME) Type 2 (R&D Systems) in kidney tumoroid medium (KOM) (Advanced Dulbecco's Modified Eagle Medium (DMEM)/F12 (Gibco) containing 1X GlutaMAX (Thermo Fisher Scientific), 10 mM HEPES (Thermo Fisher Scientific) and 1X Penicillin-Streptomycin (P/S) (Merck Millipore), supplemented with 10% R-spondin–conditioned medium, 1.5% B27 supplement (Gibco), 50 ng/mL epidermal growth factor (EGF) (PeproTech), 50 ng/mL fibroblast growth factor (FGF-)2 (PeproTech), 1.25 mM N-acetylcysteine (Sigma), 10 □M Rho-associated coiled–coil containing protein kinase (ROCK) inhibitor Y-27632 (Abmole) and 5 uM A83-01 (Tocris Bioscience))
103-T Luc	Malignant rhabdoid tumor	Gift from Jarno Drost (Utrecht); derived from 103-T wild type by lentiviral transduction with pLKO.1-UbC-luciferase blast and pLV-H2B-mNeon-puro cassettes[32,33]	None	'MRT medium'
D341 wild type	Medulloblastoma	Gift from Michael Taylor, The Hospital for Sick Children, Canada	CVCL_0018	DMEM (Gibco) + 10% FCS + 1x Glutamax (Gibco)

D341 GFP/Luc	Medulloblastoma	Derived from D341 wild type by RD114 γ-retroviral transduction with GFP/Luc	None	DMEM (Gibco) + 10% FCS + 1x Glutamax (Gibco)
D425 wild type	Medulloblastoma	Gift from Michael Taylor, The Hospital for Sick Children, Canada	CVCL_1275	DMEM (Gibco) + 10% FCS + 1x Glutamax (Gibco)
D425 GFP/Luc	Medulloblastoma	Derived from D425 wild type by RD114 γ-retroviral transduction with GFP/Luc	None	DMEM (Gibco) + 10% FCS + 1x Glutamax (Gibco)
293-T (HEK293T)	Transformed cell line	ATCC	CVCL_0063	IMDM + 10% FCS

710

711 *CAR sequences*

712 All CARs were expressed using an SFG backbone in a 2nd generation RD114 γ-retroviral
713 system. All plasmids were sequenced to verify absence of unexpected sequence mutations
714 prior to manufacture of virus. A diagram of construct structure is shown in Figure 1A, with all
715 anti-B7H3 CARs expressed in the following format: RQR8-T2A-scFv-CD8αLinker-CD8αTM-
716 CD28endodomain-CD3ζchain. The sequences for the scFv's were obtained from public
717 sources and are summarized in the below table. To insert these into the CAR backbone, the
718 scFv sequences were ordered as geneblocks and then restriction cloned into a CD8α-CD28-
719 CD3ζ format.

720

scFv ID	***Full CAR Amino Acid Sequence***	***Source of scFv Sequence***
MGA271	EVQLVESGGGLVQPGGSLRLSCAASGFTFSSFGMHWVRQAPGKGLEW VAYISSDSSAIYYADTVKGRFTISRDNAKNSLYLQMNSLRDEDTAVYYCG RGRENIYYGSRLDYWGQGTTVTVSSGGGGSGGGGSGGGGSDIQLTQS PSFLSASVGDRVTITCKASQNVDTNVAWYQQKPGKAPKALIYSASYRYS GVPSRFSGSGSGTDFTLTISSLQPEDFATYYCQQYNNYPFTFGQGTKLEI KAAADPTTTPAPRPPTPAPTIASQPLSLRPEACRPAAGGAVHTRGLDFAC DIYIWAPLAGTCGVLLLSLVITLYRTRSKRSRLLHSDYMNMTPRRPGPTRK HYQPYAPPRDFAAYRSRVKFSRSADAPAYQQGQNQLYNELNLGRREEY DVLDKRRGRDPEMGGKPRRKNPQEGLYNELQKDKMAEAYSEIGMKGER RRGKGHDGLYQGLSTATKDTYDALHMQALPPR*	Macrogenics Inc Patent 'US9441049B2'[34]; development described by Loo and colleagues[18]

376.96	EVQLVESGGGLVKPGGSLKLSCEASRFTFSSYAMSWVRQTPEKRLEWV AAISGGGRYTYYPDSMKGRFTISRDNAKNFLYLQMSSLRSEDTAMYYCA RHYDGYLDYWGQGTTLTVSSGGGGSGGGGSGGGGSDIVMTQSHKFMS TSIGARVSITCKASQDVRTAVAWYQQKPGQSPKLLIYSASYRYTGVPDRF TGSGSGTDFTFTISSVQAEDLAVYYCQQHYGTPPWTFGGGTKLEIKAAAD PTTTPAPRPPTPAPTIASQPLSLRPEACRPAAGGAVHTRGLDFACDIYIWA PLAGTCGVLLLSLVITLYRTRSKRSRLLHSDYMNMTPRRPGPTRKHYQPY APPRDFAAYRSRVKFSRSADAPAYQQGQNQLYNELNLGRREEYDVLDK RRGRDPEMGGKPRRKNPQEGLYNELQKDKMAEAYSEIGMKGERRRGK GHDGLYQGLSTATKDTYDALHMQALPPR*	University of North Carolina at Chapel Hill, General Hospital Corp Patent 'US10233226B2'[35] ; development described by Imai[19] and Sabbatino[36]
TE9	QVQLQQSGAALVKPGTSVKLSCKASGYTFTSYWMHWVKQRPGQGLEWI GMIHPKSGSVDYNEKFTNKATLTGDKSSGTAYMQLSSLTSEDSAVYYCA RGGYGSPFDYWGQGTTVTVSSGGGGSGGGGSGGGGSENVLTQSPAIM SASPGEKVTMTCSASSSVSYMYWYQQKPGSSPRLLIYRTSNLASGVPAR FSGSGSGTSYSLTISSMEAEDAATYYCQQWSSNPPTFGGGTKLEIKRAA ADPTTTPAPRPPTPAPTIASQPLSLRPEACRPAAGGAVHTRGLDFACDIYI WAPLAGTCGVLLLSLVITLYRTRSKRSRLLHSDYMNMTPRRPGPTRKHY QPYAPPRDFAAYRSRVKFSRSADAPAYQQGQNQLYNELNLGRREEYDV LDKRRGRDPEMGGKPRRKNPQEGLYNELQKDKMAEAYSEIGMKGERRR GKGHDGLYQGLSTATKDTYDALHMQALPPR*	Developed in-house at UCL. Development described by Birley *et al* [20]

721

722 <u>*CAR-T cell manufacture*</u>

723 Leukapheresis cones were acquired from NHS Blood and Transplant. PBMCs were separated
724 through Ficoll centrifugation using Lymphoprep (STEMCELL Technologies). PBMCs were
725 washed and residual red cells lysed with ACK Lysis buffer (Thermo Fisher Scientific). NK cells
726 were depleted using magnetic CD56 depletion beads (Miltenyi Biotec) and LD depletion
727 columns (Miltenyi Biotec). PBMCs were suspended in RPMI1640 containing 10% FCS and 1x
728 L-glutamine at a concentration of 1 x 10^6 cells/mL, and then activated with 0.5 mg/mL of anti-
729 CD3 (clone: OKT-3; Miltenyi Biotec) and anti-CD28 antibodies (clone: CD28.2; Miltenyi
730 Biotec). Forty-eight hours before transduction and on the day of transduction, 100 IU/mL
731 recombinant human IL-2 (Proleukin, Novartis) was added. T cells were transduced with the
732 above-mentioned γ-retroviral SFG construct following plating on retronectin (Takara Bio)-
733 coated plates and spinoculation. Transduction efficiency was measured three days after
734 transduction using flow cytometry by staining for RQR8 (clone: QBNED10; R&D BioSystems).
735 T cell populations were not corrected for transduction efficiency in functional assays.
736 Transduction efficiencies of >50% were routinely achieved. Expanding CAR-T cell IL-2 media
737 was replenished every two days. Expansions were harvested at day 10-12 following culture

738 initiation and cryopreserved in 10% DMSO complete media. When initiating *in vitro* or *in vivo*
739 functional assays, CAR-T cells were thawed in pre-warmed IL-2 (100 IU/mL) complete media
740 (RPMI1640, 10% FCS), rested overnight and then counted. CAR-T E:T ratios were based on
741 the number of viable T cells after overnight rest. Cryopreserved CAR-T recovery after
742 overnight rest (relative to the number of CAR-T that were frozen down) was routinely 50-60%,
743 with a ~90% viability.

744 *Animal studies*

745 Animal protocols were approved by local institutional research committees and in accordance
746 with UK Home Office guidelines. Mixed male and female NSG mice aged between 6 and 8
747 weeks were supplied by Charles River. All experiments were carried out under UK home office
748 licenses project license number 15981/01, and personal license numbers I13398879,
749 P2E645DD9, I83870811, I27052867, I8C20AD0D and I754094BC.

750 For the LAN-1 *in vivo* study, NSG mice were injected with 1 x 10^6 LAN-1-BFP/Luc in Matrigel
751 (Corning) subcutaneously into the flank. CAR-T cells (1 x 10^7) were injected intravenously into
752 the tail vain at day 10 following tumor engraftment (treatment schedule illustrated in Figure
753 1E). Tumor size was monitored twice a week with digital callipers. Mice were given 200 uL
754 luciferin (Thermo Fisher Scientific) into the scruff and imaged using a PhotonIMAGERTM
755 optical imaging system (Biospace Lab) weekly. Animal sacrifice was initiated upon reaching
756 either a tumor diameter of >15 mm in any direction (as measured by callipers) or the
757 appearance of tumor burden toxicity that exceeds our animal welfare standards (>15% weight
758 loss, change in activity, ataxia, dehydration, loss of normal gait, grimacing).

759 For the Med8A *in vivo* study, two types of model were run: the 'high-stress' model and the
760 'low-stress' model. In both models 5 x 10^4 Med8A cells re-suspended in PBS were injected
761 into the cerebellum of an NSG mouse. In the 'low-stress model' (illustrated in Figure 1B), two
762 days after tumor engraftment the mice were administered intraventricularly with 2.5 x 10^6 CAR-
763 T cells. In the 'high-stress model' (illustrated in Figure 1C) the mice were treated six days after

764 tumor engraftment, and with 0.5 x 10^6 CAR-T cells per animal. Mice were given 200 uL luciferin
765 (Thermo Fisher Scientific) into the scruff and imaged using a PhotonIMAGERTM optical
766 imaging system (Biospace Lab) weekly. Animal sacrifice was initiated upon reaching either a
767 tumor luminescence of 10E10 photons/second/cm^2 (via IVIS), or the appearance of tumor
768 burden toxicity that exceeds our animal welfare standards (>15% weight loss, doming of the
769 cranium, change in activity, ataxia, dehydration, loss of normal gait, grimacing).

770 *CAR-T in vitro functional assays*

771 A number of different functional CAR-T assays were performed. While high (>60%)
772 transduction efficiency of CAR-T was routinely achieved, transduced cell numbers were
773 normalised for functional assays to ensure that each binder condition receives the same
774 number of viable CAR-T cells. All data was collected in experimental duplicates or triplicates,
775 as indicated in figure legends.

776 CAR-T responses against LAN-1 and Kelly target cells were assessed as follows. For the
777 overnight (~18h) co-culture cytokine assays, CAR-T cells were co-cultured with LAN-1, Kelly
778 cells or no antigen stimulus in 48-well plates at an E:T ratio of 1:1. After 18 h, supernatant was
779 removed for ELISA and cells incubated with monensin (BioLegend). Checkpoint receptors PD-
780 1, TIM-3 and LAG-3 were detected by flow cytometry. Overnight cytotoxicity was tested using
781 a ^{51}Cr release assay. Target cells were incubated with ^{51}Cr for 1 h then washed and plated in
782 96-well plates. CAR-T cells or untransduced cells were plated at a range of E:T ratios. The
783 plates were incubated for 4 h at 37°C and then the supernatant was removed and incubated
784 with scintillation fluid (PerkinElmer) overnight at room temperature. ^{51}Cr released into the
785 supernatant was measured using a 1450 MicroBeta TriLux (PerkinElmer). For the re-
786 challenge assays, CAR-T cells were co-cultured with irradiated LAN-1, Kelly, or no target cells
787 in 24-well plates at an E:T ratio of 2:1. Cell medium was replenished every 2–3 days. CAR-T
788 cells were challenged with irradiated target cells every 6 days, cultured for a further 24 h, and
789 analyzed. Cells were pelleted and supernatant was removed every week for ELISA. CAR-T

790 cell proliferation was measured weekly by flow cytometry using Precision Count Beads
791 (BioLegend). The levels of cytokines IL-2 and IFN-γ were quantified using ELISA MAX Deluxe
792 Set Human IL-2 and ELISA MAX Deluxe Set Human IFN-γ (BioLegend).

793 SupT1-B7H3^{range} re-challenge assays were performed as follows (illustrated in Figure 6C). For
794 the overnight (~18h) co-culture cytokine assays, CAR-T cells were co-cultured with GFP/Luc-
795 SupT1-B7H3^{range} cells or GFP/Luc-SupT1-WT cells in 96-well plates at an E:T ratio of 1:1.
796 After 18 h, supernatant was removed for analysis with ELISA MAX Deluxe Set Human IL-2
797 and ELISA MAX Deluxe Set Human IFN-γ (BioLegend). Cytotoxicity at the various indicated
798 timepoints was tested using a luciferase-based assay. Briefly, 15ug/mL of D-luciferin (Perkin
799 Elmer) was added to each well to document the remaining number of living tumor cells. The
800 plate was then incubated for 5 min at 37°C in 5% CO_2 and run on a SpectraMax, Molecular
801 Devices analyzer, with 'no effector' tumor wells as controls for T cell-mediated tumor death.
802 CAR-T cells or untransduced cells were plated at a 1:1 E:T ratio, with daily re-challenges.
803 Cytotoxicity readings were done in this manner 18h after each new tumor re-stimulation. CAR-
804 T cell proliferation was measured weekly by flow cytometry using Precision Count Beads
805 (BioLegend).

806 Brain tumor challenge assays with GFP/Luc-Med8A, -D425 and -D341 cells were done by
807 plating CAR-T cells with targets at the indicated E:T ratios in 96-well plates. Cytotoxicity at
808 96h following tumor challenge was tested using a luciferase-based assay. Briefly, 15ug/mL of
809 D-luciferin (Perkin Elmer) was added to each well to document the remaining number of living
810 tumor cells. The plate was then incubated for 5 min at 37°C in 5% CO_2 and run on a
811 SpectraMax, Molecular Devices analyzer, with 'no effector' tumor wells as controls for T cell-
812 mediated tumor death. CAR-T cell proliferation was measured weekly by flow cytometry using
813 Precision Count Beads (BioLegend).

814 Malignant rhabdoid tumoroids were established, characterised and cultured as previously
815 described[30,31]. 103-T tumoroids were transduced with a construct encoding for luciferase were

816 cultured in KOM in BME droplets for 7 days in advance. 4 days before the co-culture the
817 tumoroids were disrupted mechanically into a single cell suspension by mechanical
818 dissociation and seeded in BME droplets. On the day of CAR-T challenge, MRT tumoroids
819 were collected, washed with cold medium to remove BME, and a fraction was dissociated into
820 a single cell suspension. Single tumor cells were counted to determine the number of cells
821 present in the MRT tumoroid suspension. MRT tumoroids were then seeded out with an
822 equivalent of 7500 single tumor cells per well in 50 uL of co-culture medium containing 10%
823 FBS and a 1:1 ratio of KOM and RPMI with 1X GlutaMAX and 1X P/S. To determine tumor
824 specific killing, a released luciferase assay was performed using the luciferase assay system
825 (Promega). Medium was removed and cells were washed with 100 uL of PBS. 20 uL of 1X
826 passive lysis buffer (Promega) were added and the plate was incubated at room temperature
827 for 15 min while shaking. In a LUMITRAC white polystyrene 96-well plate (Greiner) 100 uL of
828 the luciferase reagent were added to 20 uL of the lysed cells and the plate was measured at
829 the FluoSTAR Omega Microplate reader immediately. Luciferase signal was determined on
830 day 1 after co-culture as well as before re-challenge with new tumoroids.

831 To measure CAR-T cytotoxicity against (AMC) 691-B and 691-T neuroblastoma tumoroids,
832 GFP-Luc tumoroids were dissociated into single cells by re-suspending in 1 mL of Accutase
833 solution (Sigma-Aldrich) through a p10 tip on top of a p1000 tip to combine both enzymatic
834 and mechanic dissociation methods. Tumoroid cells in suspension were counted and plated
835 two days before the beginning of the experiment to ensure spheroid formation in 96-well white
836 flat bottom plates(Costar). On the day of initiation co-culture, CAR-T cells were counted and
837 plated with GFP/Luc tumoroids at the stated E:T ratios in half 'neurosphere medium'
838 (expanded on in the Cell Lines section of Methods and Materials) and half T cell medium
839 (RPMI- GlutaMAX 1640 + 25 mM Hepes (ThermoFisher) supplemented with 10% FCS
840 (Gibco), 1% penicillin/streptomycin (ThermoFisher) and 1% L- glutamine (ThermoFisher)
841 supplemented with 100 IU/mL IL-2 (Miltenyi Biotec)). For re-challenge, tumoroids were plated
842 2 days before each challenge, with the CAR-T culture added on top. Tumoroid re-challenge a

843 set E:T ratio was done every 2-3 days. Cytotoxicity was measured by adding 15ug/mL of D-
844 luciferin (Perkin Elmer) to each well to document the remaining number of living tumor cells,
845 with 'no effector' tumor wells as controls for T cell-mediated tumor death. Cells were then
846 incubated for 5' at 37°C in 5% CO_2 and readout performed in the FLUOstar Omega microplate
847 reader.

848 *Flow cytometry staining and analysis*

849 The following cell cytometers were used to collect flow cytometry data: BD ® LSR II Flow
850 Cytometer (BD Biosciences), FACSymphony™ A5 High-Parameter Cell Analyzer (BD
851 Biosciences) and CytoFLEX S V4-B2-Y4-R3 Flow Cytometer (Beckman Coulter). FlowJo
852 10.9.0 software for Mac (Becton Dickinson) was used to analyse flow cytometry data. All
853 staining was done in FACS buffer, PBS, 2% FCS with 2mM EDTA. Samples were either
854 analysed immediately following staining or fixed with Biolegend Fixation Buffer and analysed
855 within two weeks. The following table lists the flow cytometry staining reagents that were used:

856

Target	***Product ID***	***Catalogue Number***
Viability Dye	Fixable Blue Dead Cell Stain — LIVE/Dead™ (Thermo)	L34961
Flow count beads	Precision Count Beads (Biolegend)	424902
B7H3-his	B7H3-his protein to detect CAR at the cell surface (R&D Biosystems)	1949-B3-050/CF
His	Anti-his mAb clone J095G46-APC (BioLegend)	362605
Ag Density Quantification	BD Biosciences™ Quantibrite™ Phycoerythrin (PE) Beads; used to quantify B7H3 antigen density on target cell surface	10626384
Fixation buffer	Fixation buffer (Biolegend)	420801
Cell membrane dye	eBioscience Cell Proliferation Dye eFluor 450 (blue) (Thermo Fisher); used to label cells for BEHAV3D analysis	65-0842-85

Cell membrane dye	Calcein AM (green) (Thermo Fisher); used to label cells for BEHAV3D analysis	C1430
Cell membrane dye	CellTrace™ Far Red Cell Proliferation Kit, for flow cytometry; used to label cells for Lumicks z-Movi analysis	C34564
RQR8 marker gene	Clone QBEND10-APC (BioTechne)	FAB7227A
CD3	Clone OKT-3-Brilliant Violet 711 (Biolegend)	317328
CD4	Clone VIT4-VioBlue (Miltenyi Biotec),	130-113-219
B7H3	Clone MIH42-PE (BioLegend)	351003
PD-1	Clone EH12.1-Brillant Violet 605 (Beckton Dickinson)	563245
CD25	Clone 2A3-Briljant Violet 711 (Beckton Dickinson)	563159
CD4	Clone A161A1-FITC (Biolegend)	357406
CD8	Clone SK1-PerCP (Biolegend)	344706
TIM-3	Clone F38-2E2-PE (Biolegend)	345006
CCR7	Clone G043H7-PE/Dazzle594 (Biolegend)	353235
CD69	Clone FN50-PE-Cy7 (Beckton Dickinson)	561928
CD137	Clone 4B4-1-APC (Beckton Dickinson)	550890
CD3	Clone HIT3a-Alexa Fluor 700 (BioLegend)	300324
CD45RA	Clone HI100-APC/Cy7 (Beckton Dickinson)	750258

857

858 *Lumicks CAR-T synapse avidity measurements*

859 Proprietary z-Movi Lumicks protocols were followed under the supervision of Lumicks staff
860 present for the assays. Briefly, SupT1-WT, SupT1-B7H3^{hi}, LAN-1 and Med8A tumor cells were
861 seeded in a z-Movi microfluidic chip (Lumicks, Amsterdam, Netherlands) coated with poly-L-
862 lysine and cultured for 16 hours. The next day, flow sorted, transduction efficiency-normalized
863 and CellTrace Red (Biolegend)-labelled CAR-T cells were serially flowed in the chips and
864 incubated with the target cells for 10 minutes prior to initializing a 3-minute linear force ramp.
865 During the force ramp, the z-Movi device (Lumicks) captured a time series of images using a
866 bright field microscope integrated into the platform. Detached cells were levitated towards the
867 acoustic nodes, allowing the tracking of cells based on their XY positions. Changes in the Z-
868 position resulted in a change in the diffraction pattern, which allowed the distinction between
869 cells adhered to the substrate and cells suspended to the acoustic nodes. This information
870 was used to correlate cell detachment events with a specific rupture force. Cell detachment
871 was acquired using z-Movi Tracking and post experiment image analysis was done using Cell
872 Tracking offline analysis. Data were presented as 'mean % CAR-T attached cells' at the
873 maximum mean force applied, 1000 piconewtons, pN. This was repeated in experimental
874 triplicate for four biological T cell donors. A greater depth of z-Movi workflow is reported
875 online[37]. The software used to acquire the data was z-Movi Software (v1.0).

876 *Binder affinity measurements*

877 Biacore surface plasmon resonance (SPR) for anti-B7H3 antibodies was done as previously
878 described[38]. Briefly, MGA271, 376.96 and TE9 binders were expressed in human IgG1 format
879 (Evitria), and then evaluated by Antibody Analytics using Biacore SPR for binding kinetics to
880 4-Ig human B7H3. Anti-B7H3 antibodies were first adhered to plates and several
881 concentrations of Human B7-H3 analyte were passed over the surface to assess the binding
882 interactions. The data is shown in Figure 2G. Clone 9G8 mAb was used as an isotype control.

883 *BEHAV3D CAR-T / tumoroid imaging*

884 Tumoroids (691-B and -T) were grown in 'Neurosphere medium' (as described in the 'Cell
885 Lines' section), cultured for 3 weeks prior to the experiments and passaged once or twice a
886 week according to tumoroid size and confluence. The experimental timeline is illustrated in
887 Figure 7A. CAR T cells were thawed one day prior to the start of the experiment in RPMI-
888 GlutaMAX 1640 + 25 mM Hepes (ThermoFisher) supplemented with 10% FCS (Gibco), 1%
889 penicillin/streptomycin (ThermoFisher) and 1% L- glutamine (ThermoFisher), rested overnight
890 at a density of $1x10^7$ cells/mL in 100 IU/mL IL-2 (Miltenyi Biotec)-supplemented medium. CAR
891 T cells for the initial challenge day 0 imaging experiment were stained with the following
892 antibody mix in FACS buffer (PBS 1x + 2% FCS + 2mM EDTA): anti-RQR8 mAb clone
893 QBEND10-APC (R&D Systems), anti-CD4 mAb clone VIT4-VioBlue (Miltenyi Biotec) and
894 mouse serum (Invitrogen). $RQR8^+CD4^+$ and $RQR8^+CD4^-$ CAR-T cells were FACS-sorted with
895 a Sony SH800S cell sorter into FCS, and rested overnight in a density of $1x10^7$ cells/mL in
896 medium supplemented with 100 IU/mL IL-2 (Miltenyi Biotec).

897 For co-culture experiments, tumoroids were dissociated into single cells by pipetting 1 mL of
898 Accutase solution (Sigma-Aldrich, counted and plated two days before the beginning of the
899 experiment to ensure spheroid formation in either 12-well flat-bottom plates (for rec-hallenges)
900 (Greiner) or in a glass-bottom 96-well SensoPlate (Greiner) for imaging. The correct cell
901 number was determined considering organoid growth rates. Wild type organoids were used.
902 Sorted and rested CAR T cells were stained separately with eBioscience Cell Proliferation Dye
903 eFluor 450 (1:4000, ThermoFisher) or Calcein AM (1:3000, ThermoFisher) in PBS for 15
904 minutes at 37°C and mixed in a 1:1 ratio immediately before plating them with the organoids
905 in a 1:5 E:T ratio. The co-culture medium (100µL organoids + 100µL T cells) was then
906 supplemented with 2.5% basement membrane extract (BME, Cultrex), Nucred Dead 647
907 (three drops per mL, ThermoFisher), and TO-PRO-3 (1:5000, ThermoFisher). The
908 combination of Nucred Dead 647 and TO-PRO-3 has previously been described by Dekkers
909 et al[24]. The plate was placed in a SP8 confocal microscope (Leica) containing an incubation
910 chamber (37°C, 5% CO2) and imaged for thirteen hours in time series with two-minute

911 intervals (as shown in Supplementary Figure 10). Day 7 BEHAV3D imaging was the third
912 challenge with 691 tumoroids. On Day 6, cells from re-challenge plates were stained with the
913 following antibody mix in FACS buffer (PBS1x + 2% FCS + 2mM EDTA): anti-RQR8 mAb
914 clone QBEND10-APC (R&D Systems), anti-CD4 mAb clone VIT4-VioBlue (Miltenyi Biotec),
915 anti B7H3 mAb clone MIH42-PE (BioLegend) and mouse serum (Invitrogen). $B7H3^-$
916 $CD34^+CD4^+$ and $B7H3^-$ $CD34^+CD4^-$ CAR-T cells were FACS-sorted with the Sony SH800S
917 cell sorter into FCS, rested overnight at a density of $1x10^7$ cells/mL in medium supplemented
918 with 100 IU/mL IL-2 (Miltenyi Biotec). On day 7, rested CAR-T cells were stained separately
919 and plated with WT organoids in a 1:5 E:T ratio, as described above. The plate was placed in
920 a SP8 confocal microscope (Leica) containing an incubation chamber (37°C, 5% CO2) and
921 imaged for thirteen hours in time series with a two-minute interval.

922 Image processing was done according to the protocol previously described by Dekkers *et al*[24]
923 using the Imaris (Oxford Instruments) version 10.0 software for 3D visualization, cell
924 segmentation and extraction of statistics. The Channel Arithmetics Xtension was used to
925 create additional channels for the specific identification of $CD8^+$ and $CD4^+$ T cells (live and
926 dead), organoids (live and dead), and to exclude debris. The Surface and ImarisTrack
927 modules were used to specifically detect and track T cells and/or organoids. For tracked T
928 cells, time-lapse statistics consisting of the coordinates of each cell, speed, square
929 displacement, distance to either organoids or the other T cell subset, and dead cell dye
930 channel intensity were exported into a metadata file for subsequent processing and analysis.

931 *Data presentation*

932 Data was graphed and analysed statistically using Graphpad Prism 10 for macOS software
933 (Dotmatics). Statistical tests were chosen as suitable to particular data sets, and statistical test
934 recommendations by Graphpad Prism 10 software were followed, based on data type,
935 replicates and degree of pairing. The number of biological and experimental replicates used
936 in each analysis is listed in respective figure legends. Data processing for the BEHAV3D

platform was done using ‘R’ programming language code that was written by and published from the Rios group[24].